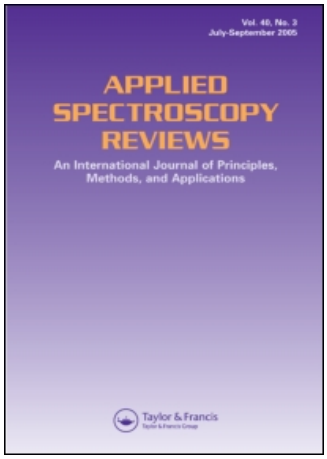

Applied Spectroscopy Reviews
Publication details, including instructions for authors and subscription information:
http://www.informaworld.com/smpp/title~content=t713597229

The Molecular Architecture of Lipid Membranes - New Insights from Hydration-Tuning Infrared Linear Dichroism Spectroscopy

Hans Binder [a]
[a] Interdisciplinary Centre for Bioinformatics, University of Leipzig. Leipzig. Germany

First Published on: 03 March 2003
To cite this Article: Hans Binder , 'The Molecular Architecture of Lipid Membranes - New Insights from Hydration-Tuning Infrared Linear Dichroism Spectroscopy', Applied Spectroscopy Reviews, 38:1, 15 - 69
To link to this article: DOI: 10.1081/ASR-120017480
URL: http://dx.doi.org/10.1081/ASR-120017480

MARCEL DEKKER, INC. • 270 MADISON AVENUE • NEW YORK, NY 10016

APPLIED SPECTROSCOPY REVIEWS
Vol. 38, No. 1, pp. 15–69, 2003

The Molecular Architecture of Lipid Membranes—New Insights from Hydration-Tuning Infrared Linear Dichroism Spectroscopy

Hans Binder*

University of Leipzig, Interdisciplinary Centre for Bioinformatics, Leipzig, Germany

CONTENTS

*Correspondence: Dr. Hans Binder, University of Leipzig, Interdisciplinary Centre for Bioinformatics, Kreuzstr. 7b, D-04103 Leipzig, Germany; Fax: ++49-341-14951-19; E-mail: binder@rz.uni-leipzig.de.

DOI: 10.1081/ASR-120017480 0570-4928 (Print); 1520-569X (Online)

MARCEL DEKKER, INC. • 270 MADISON AVENUE • NEW YORK, NY 10016

MARCEL DEKKER, INC. • 270 MADISON AVENUE • NEW YORK, NY 10016

ABSTRACT

A new, precise method of adjustment and variation of the hydration degree of materials, is presented. This humidity-titration technique has proved to be practical, relatively fast to achieve, accurate, and, last but not least, well-defined in a thermodynamic sense. It is used in combination with infrared (IR) attenuated total reflection (ATR) spectroscopy to study the hydration of selected phospholipids on a molecular level. Examples of hydration-driven, lyotropic phase transitions are presented and discussed. The second part of the article deals with the relationship between polarised IR absorption spectroscopy and the degree of molecular order in macroscopically oriented samples. The basic formulae for the analysis of IR dichroism data in terms of molecular order parameters are given. Aspects of the molecular order of lipid membranes, such as the orientation and conformation of phosphocholine (PC) headgroups before and after interaction with ions (Ca^{2+} and Mg^{2+}), the segmential order of the acyl chains in fluid and solid phases, complex formation between water and the PC headgroups and the ordering of lipid-bound water are presented in the third part of this publication. These examples illustrate the effect of the hydration degree on the molecular architecture of lipid assemblies.

Key Words: ATR technique; Humidity titration; Lyotropic phase behavior; Molecular order; Phospholipid bilayer; Headgroup orientation.

I. INTRODUCTION

Water is a fascinating small molecule because of its unique properties: it can establish two hydrogen bonds and at the same time accept two other hydrogen bonds. These properties enable water to interact with neighbouring molecules in many different ways with far-reaching consequences for the physico-chemical properties of many materials. It may completely modify the conformation and interactions of biomacromolecules making hydration an important factor that influences their biological function. Biological relevant molecules are often either hydrophobic tending to separate from water (hydrophobic effect) or they are hydrophilic with the tendency to solvate. A third, important class includes molecules, which are composed of hydrophilic and hydrophobic parts making them amphiphilic (or amphipatic). Upon hydration these molecules typically assemble into aggregates, which are characterised by polar and apolar regions of microscopical dimensions. The mode of water

MARCEL DEKKER, INC. • 270 MADISON AVENUE • NEW YORK, NY 10016

binding affects structure and dynamics of the aggregates. Many lipids form bilayer membranes in an aqueous environment. These lamellar structures attract considerable interest because they represent the basic structural unit of cellular membranes.

The molecular packing and chain organisation, as well as the bilayer topology, and the interactions between bilayers depend on the amount of water associated with the polar headgroups of the lipids. The association of water molecules with lipids constitutes therefore one fundamental aspect of biomembrane structure and function.

Infrared (IR) spectroscopy has been proved to probe the conformation, environment and dynamics of complex amphiphilic systems on a molecular level.[4] Furthermore, IR absorption of ordered molecular assemblies possesses usually linear dichroism, which manifests molecular orientations spectroscopically.[5] It was used to characterise crystals of paraffins and fatty acids[6] and also liquid crystalline and polymeric materials.[7,8] The so-called Attenuated Total Reflection (ATR) technique[9] has been applied to study lipid ordering in membranes since the pioneering work of Fringeli and Günthard.[10–17]

The present paper summarises new aspects of hydration studies on lipid assemblies: The so-called humidity titration technique is presented in the first part. It enables adjustment and variation of lipid hydration with high precision. Selected examples illustrate the effect of water adsorption on the structure and phase behavior of lipid systems. The second part focusses on methodical aspects of linear dichroism measurements using the ATR technique. This method was applied to characterise the molecular architecture of lipid membranes. Selected results were presented in the third part of this publication.

II. HYDRATION-TUNING INFRARED SPECTROSCOPY

A. Adjustment of the Hydration Degree of Materials

Many amphiphiles exhibit a rich structural polymorphism depending on the nature of the molecules, their hydration degree, and on external conditions given by means of temperature and pressure. The temperature can be easily adjusted and controlled in physico-chemical experiments. As a result, thermotropic (temperature dependent) studies are frequently realised. Temperature, however, suffers from the disadvantage that changes of this variable result in simultaneous alterations in volume, intermolecular interactions and thermal energy, which makes it difficult

MARCEL DEKKER, INC. • 270 MADISON AVENUE • NEW YORK, NY 10016

to disentangle these contributions. Alternatively, one can vary the external (hydrostatic) pressure at a constant temperature.[18–21] Such barotropic experiments permit the isolation of effects that depend on changes in density. Consequently, this method provides a direct approach to molecular interactions, which depend directly on intermolecular distances and molecular conformations.

As a third option one can modulate the properties of amphiphilic systems by alteration of their hydration degree. Such lyotropic experiments provide a direct access to assessing the role of water for the stability and structure of molecular aggregates. Moreover, the hydration degree represents an independent thermodynamic degree of freedom, and its variation opens up novel opportunities to study physico-chemical properties of amphiphilic molecules such as lipids. Note, hydration studies provide information not only on water binding properties, but they are also able to probe elastic properties of amphiphilic aggregates[22–24] and phase behavior.[2,25] Lyotropic phase transitions between lamellar and non-lamellar, solid gel or subgel and liquid crystalline phases reveal microscopic characteristics such as preferred shape, flexibility/rigidity and hygroscopicity of the molecules and the intermolecular forces acting between them on a macroscopic level.

There are two types of thermodynamic variables that characterise the hydration degree of a system: (i) The amount of water given in concentration units such as its volume fraction or the molar ratio water-to-amphiphile, $R_{W/L}$, and (ii), the ''hydration strength of water'' given in terms of water activity, $0 \leq a_w \leq 1$. The minimum and maximum values, $a_w = 0$ and 1, refer to the dry system and to bulk water, respectively.

Accordingly, the hydration degree of a sample can be adjusted in two different ways: (i) Water and amphiphile are mixed in appropriate amounts, or (ii), the sample is brought in thermodynamic equilibrium with a reservoir of definite water activity. In the latter case, hydration water, which is associated with the amphiphiles possesses the same activity as water in the reservoir after equilibration.

An aqueous polymer solution can serve as the reservoir. It typically provides water activities greater than 0.9 in dependence on the polymer concentration.[22,23,26] Alternatively, one can expose the sample to an atmosphere of constant relative humidity, $\mathrm{RH} \equiv a_W \cdot 100\% = p/p_s \cdot 100\%$ where p and p_s denote the partial pressure of water in the gas and the partial pressure of saturated water vapour, respectively. This method is suited for samples with a sufficiently large surface that enables water adsorption via the gas phase and distribution of the sorbent (water) in the sorbate (amphiphile) by diffusion. Amphiphiles and other materials such as powders and porous solids in most cases meet these conditions.

B. Step-by-Step and Dynamic Measurements

An atmosphere of a certain RH value can be simply realised by means of saturated aqueous salt solutions. For example, one obtains the series RH $\approx$ 12% (LiCl), 32% ($MgCl_2$), 58% (NaBr), 75% (NaCl), 84% (KCl), 92% (KNO_3) and 97% (K_2SO_4) at room temperature.[27] The conditions of saturated vapour and of dry gas may be adjusted with pure water (RH = 100%) and with phosphor pentoxide (RH = 0%). Small vessels containing these substances were placed into the thermostated and thoroughly-sealed sample chamber. For investigations in saturated vapour atmosphere ($R = 100\%$) we used water-saturated filter paper to increase the surface, which emanates the vapour. Equilibration takes from a few minutes to tenths of hours depending on the target RH, the internal volume of the sample chamber and the water-emanating surface.[28] Evaporation, diffusion and convection of the vapour inside the sample chamber, and only to a less extent the sorption of water to the sorbate, have been proved to be the rate limiting processes for equilibration in many situations.

Before each alteration of the RH, the experimentator has to open the sample chamber, to replace the reference solution by a new one and this way to start new equilibration. This technique allows to adjust at most 2–3 RH values per day. Due to these limitations, only a small number of RH points (typically 5–10) were studied in one hydration experiment. It's worth noting that many biological materials rapidly decompose within a few hours or days. Moreover, subtle hydration-induced effects, such as lyotropic phase transitions, may easily pass unoticed. Last but not least, the resolution along the RH axis remains relatively uncertain.

An alternative method utilizes the continuous change of RH during equlibration and records hydration properties as a function of time after changing the reference solution.[28,29] These dynamic measurements provide a series of data points, which correspond to a progressively varied hydration degree of the sample until it reaches equilibrium. The nonstationary values of water activity, and/or, of sample composition, were either unknown, or they were indirectly deduced from calibration experiments or on the basis of thermodynamic[29] and spectral characteristics.[28]

Dynamic measurements yield reasonable results if the sample reaches quasi-equilibrium at each nonstationary value of RH. Problems will arise if hydration-induced structural rearrangements on a molecular or mesoscopic lengthscale proceed relatively slowly.[30,31] In this case, the results of dynamic measurements may turn out to be distorted by the swelling kinetics of the sample.

MARCEL DEKKER, INC. • 270 MADISON AVENUE • NEW YORK, NY 10016

C. The Humidity Titration Technique

A third method uses the permanent flow of a chemically inert gas (nitrogen or argon), which is moistened to a defined water activity by means of a humidity/moisture generator. The gas of accurately adjusted RH and temperature (T) is led through the sample cell to perfuse the material of interest. A typical experiment runs under computer control to realise a ''humidity staircase'', i.e., the stepwise variation of RH at certain time intervals. The increase (decrease) in RH initiates the adsorption (desorption) of water onto (from) the sample film. Our technique has been called humidity titration technique because ''gaseous water'' is ''injected'' in definite portions of RH into the sample chamber.[32]

This conditioning method includes several advantages for the study of hydration phenomena: (1) It avoids intrinsic equilibration problems because the target RH value can be held constant for a sufficiently long interval until the system reaches equilibrium. (2) The water activity can be freely adjusted to any value between dryness and the (nearly) fully hydrated state ($0\% < RH < 99\%$). Consequently, the data points can be set with high density to detect subtle hydration-induced phenomena. If necessary, the degree of hydration of the sample can be varied quasi-continuously. (3) The water activity is settled and changed by means of a regulating circuit, which includes a computer, sensors and Peltier elements. This technique allows automatically to record hydration-dehydration curves at different temperatures , and thus most effectively to establish RH-T phase diagrams. (4) The continuous flow of moist gas over the sample accelerates equilibration. Hydration scans of 20–30 data points ranging from $RH = 2$ to 98% can be realised within 15–30 h. (5) Renunciation of chemicals (salt solutions) simplifies the performance of the experiment.

In summary, the adjustment of the hydration degree of materials by means of the humidity titration technique has proved to be practical, relatively fast to achieve, accurate, and, last but not least, well-defined in a thermodynamic sense (see below).

D. ATR-Infrared Spectroscopy at Variable Hydration

Infrared spectroscopy is particularly sensitive to hydration-induced effects such as the solvation of polar groups and conformational changes in the hydrophobic region of amphiphilic aggregates. Unfortunately, this method is hampered by the strong absorbance of water leading to saturation of absorption especially in the mid infrared spectral region.

This effect ruins desirable possibilities to study highly diluted samples in the transmission mode. On the other hand, a hydrated sample becomes sufficiently transparent for IR light if one succeeds to reduce the sample thickness to a few hundreds of nanometers.

These conditions can be realised by applying the ATR technique, which is based on the effect of attenuated total reflection (see below). This method is suitable for hydration studies because the absorption of light is limited to a very thin layer adjacent to the reflecting surface. Moreover, the sample can be prepared in most cases as a cast film on the ATR crystal. One side of the film faces towards the moist atmosphere. The dimensions of the film in parallel direction to the surface (millimeters to a few centimeters) exceed its thickness (several micrometers) by more than four orders of magnitude. Hence, the sample possesses a large surface, which ensures effective hydration via sorption of water from the gas phase.

ATR infrared measurements—combined with the humidity titration technique—is well suited to explore hydration-induced phenomena in amphiphilic systems. Figure 1 schematically illustrates the set-up used in our laboratory. We also adapted other analytic techniques, such as X-ray diffraction, gravimetry and sorption calorimetry, to sample conditioning by means of humidity titration in order to get supplementary information about structural, thermodynamic and stochiometric aspects of water binding.[24,30,32–34]

Figure 2 shows two series of IR spectra of the lipid 1-palmitoyl-2-oleoyl-phosphatidylcholine (POPC), which was progressively hydrated either in a H_2O or a D_2O atmosphere. The water molecules, which associate with the lipid upon increasing RH, absorb light at characteristic IR frequencies. The most intense IR bands due to the O–H and O–D stretches, are centred near $3400\,cm^{-1}$ (H_2O) and $2490\,cm^{-1}$ (D_2O). At isothermal conditions, their integrated absorbance provides a suited measure of the amount of water sorbed to the lipid, $R_{W/L}$, as has been proved by comparison with gravimetric data (see Fig. 2 and Ref.[35] for details). The marked shift of the mean frequencies of IR modes due to the C=O and PO_2^- stretches reflect changes of the degree of hydrogen bonding to the polar groups as a function of RH. Hence, IR spectroscopy is capable to characterise the overall hydration degree as well as the ''local'' hydration properties.

E. Hydration Characteristics of Selected Phospholipids

In Fig. 3 we compare the adsorption isotherm ($R_{W/L}$), and the centre of gravity of absorption bands due to vibrations of the phosphate group

MARCEL DEKKER, INC. • 270 MADISON AVENUE • NEW YORK, NY 10016

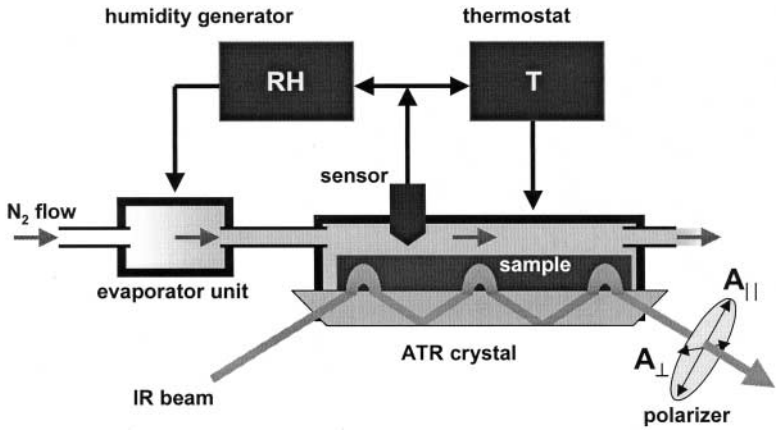

Figure 1. Schematic representation of the setup of the hydration-tuning infrared experiment. The sample thickness does not refer to scale. The ATR crystal is built into a holder unit, which realises definite values of relative humidity (RH) and temperature (T) at the crystal surface coated with the sample. The unit had been covered with a thermostated (flowing water) copper block forming a closed atmosphere above the crystal. The block was supplemented with gas influx and outflux lines and with sensors measuring the RH (capacitive RH sensor) and temperature (Pt-100 thermocouple) within the sample compartment. During the measurement, nitrogen gas of definite humidity and temperature flows through the cell (~100 mL/min). The relative humidity of the N_2-inflow had been adjusted in a humidity generator (HumiVar, Leipzig) by means of subtle water evaporation regulated with Peltier elements. The regulating circuit includes also the RH sensor and a microcomputer. The humidity generator allows to settle the RH to any value between 2% and 98% with an accuracy of ±0.5% in the temperature range of 5–45°C (±0.1 K).

and of the methylene chains, namely the antisymmetric PO_2^- and the symmetric CH_2 stretching vibrations of different diacyl-lipids with phosphatidylcholine (PC) headgroups, of methyl PC (MePC) and of dioleoyl phosphatidylethanolamine (DOPE). Despite their identical headgroups, the PC compounds are showing quite different water sorption isotherms. All PC lipids form bilayers at the conditions used. The mean frequency of the symmetrical methylene stretching band, $COG(\nu_s(CH_2))$, correlates with the conformational state of the methylene chains in the membranes. The sharp increase of the $COG(\nu_s(CH_2))$ value of DODPC, DLPC and DMPC in the intermediate RH range shows that the ordered all-trans conformation of the chains becomes distorted by gauche defects. Consequently, the

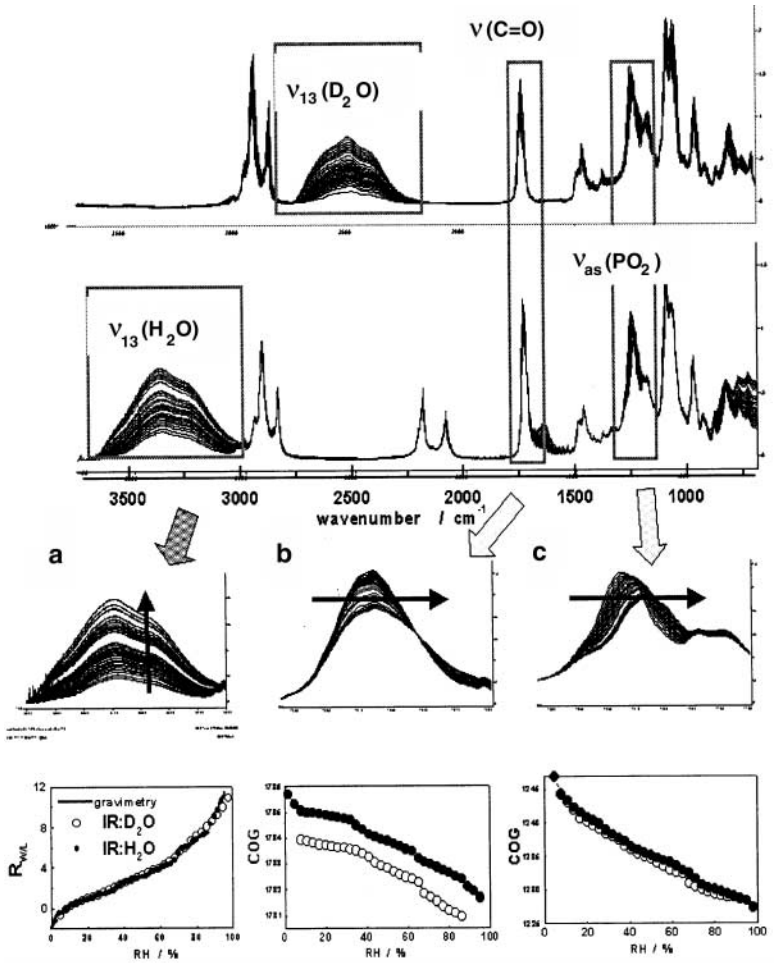

Figure 2. Characterisation of lipid hydration by means of IR spectroscopy. The IR spectra correspond to 1-palmitoyl-2-oleoyl-phosphatidylcholine (POPC, above) and its chain perdeuterated analogue POPC-d31 (below), which were hydrated in a D_2O and H_2O atmosphere, respectively. The spectra were recorded at increasing values of the relative humidity (RH) in the sample cell. The RH increment was 3%. Selected spectral regions, due to IR active modes of water (part a) and the carbonyl (part b) and phosphate (part c) groups of the lipid, were enlarged to indicate hydration-induced alterations. The absorbance of the O–H stretching mode provides a measure of the molar ratio water-to-lipid, $R_{W/L}$, of water sorbed to the lipid. The center of gravity, COG, of the carbonyl and phosphate stretches shift to smaller wavenumbers upon increasing RH because of progressive formation of hydrogen bonds to the water.

MARCEL DEKKER, INC. • 270 MADISON AVENUE • NEW YORK, NY 10016

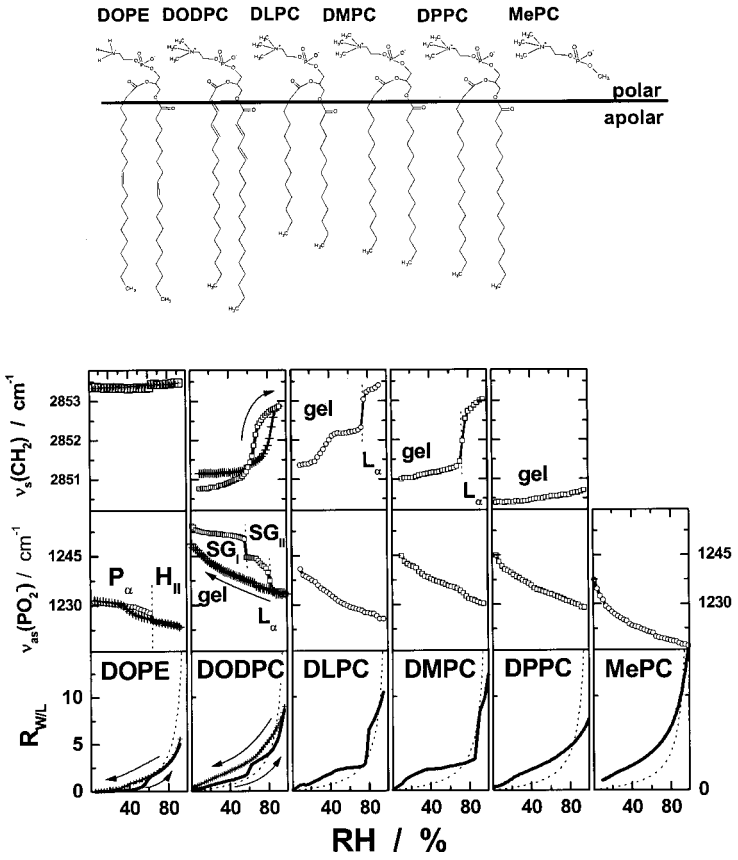

Figure 3. Hydration characteristics of different lipids as a function of the relative humidity, RH: adsorption isotherm of water (below, $R_{W/L}$ denotes the molar ratio water-to-lipid), center of gravity of the antisymmetrical phosphate stretching mode, $\nu_{as}(PO_2^-)$ and center of gravity of the symmetrical CH_2 stretching vibration (above). The data correspond to dioleoyl phosphatidylethanolamine (DOPE, $T = 25^\circ C$), dioctadecadienoylphosphatidylcholine (DODPC, $T = 25^\circ C$), dilauroyl PC (DLPC, $T = 15^\circ C$), dimyristoyl PC (DMPC, 35°C), dipalmitoyl PC (DPPC, 25°C) and methyl PC (MePC, 25°C). The dotted lines in the $R_{W/L}$ plots correspond to ideal mixing behaviour (see Eq. (2.2)).

observed sigmoidal shift of this parameter represents a characteristic signature of the chain melting transition. This event is accompanied by the significant sorption of water (compare with $R_{W/L}$) showing that structures with fluid, partly disordered chains imbibe more water than

membranes with frozen, more ordered chains. This difference can be rationalised in terms of the bigger free volume in the polar part of fluid structures, which promotes the binding of water molecules. The polar molecule MePC is capable to hydrate without constraints imposed by the presence of a hydrophobic part. Consequently, this polar compound adsorbs more water than the PC lipids at a given RH.

Figure 3 also illustrates that subtle differences in the chain packing mode strongly affect the hydration characteristics of the PC lipids in their solid state. The diene groups of DODPC induce a dense, stable packing of the octadecadienoyl chains at low and intermediate RH, which considerably impedes the binding of water compared with the other PCs that exist in the gel state at these conditions.[25,31,36] These results indicate that the phase state and the particular packing of the molecules are strongly affected by the nature of the acyl chains, which, in turn, modify the potency of the system to bind water.

The phosphate groups represent the primary hydration site of phospholipids. The mean frequency of the $\nu_{as}(PO_2^-)$ phosphate vibration of most of the PCs continuously shifts downwards with increasing RH due to the progressive formation of H–bonds to the water. This spectral parameter is hardly affected by the chain melting transition of the respective lipid except for DODPC. In this case, the stepwise alteration of $COG(\nu_{as}(PO_2^-))$ was assigned to a so called solvation-induced phase transition, an event at, which the conformation and orientation of the PC groups are changing distinctly.[3,30,36] The smallest $COG(\nu_{as}(PO_2^-))$ value among the PC compounds has been observed for MePC. This result can be explained by the higher accessibility of the phosphate oxygens of MePC for water (vide supra).

The ammonium groups of PE act as ligands for H-bonds in addition to water. Consequently, the degree of H-bonding to the PE phosphates exceeds that of PC phosphates. The smaller $\nu_{as}(PO_2^-)$ frequency of DOPE, compared with that of the PCs, reflects this difference (cf Fig. 3). On the other hand, the C=O stretching frequency of PE lipids is typically bigger than that of PCs indicating the weaker hydration of the carbonyl groups.[2,37]

One special advantage of humidity-tuned infrared spectroscopy should be recognized in its capacity for a parallel investigation of several aspects of lipid hydration. Information about intermolecular interactions, conformational changes and other structural aspects in different parts of the molecules could be studied within a given experiment.

MARCEL DEKKER, INC. • 270 MADISON AVENUE • NEW YORK, NY 10016

F. Hystereses

Series of infrared measurements were typically realised by means of increasing (hydration scan) and decreasing (dehydration scan) RH. Before measurement the sample was allowed to equilibrate for a certain time (typically 10 min) after reaching the prescribed RH in each step of the humidity "staircase." The absence of significant hysteresis effects between hydration and dehydration scans confirms that the sample reached equilibrium at each RH value. This situation was usually found in fluid systems and at the fluid/gel phase transitions.

Transitions between fluid and crystalline phases, such as the "subgel" phases of DODPC, were frequently accompanied by marked hystereses between hydration and dehydration scans, which remained unchanged when the scans were slowed down by a factor two or even more (cf Fig. 3, DODPC). The subgel phases were characterised by the rigid packing of the acyl chains. Hystereses were also found for solvation induced phase transitions. Here, direct interactions between the headgroups were broken up by water–headgroup interactions (cf Fig. 3, DOPE). The formation of a weakly hydrated crystalline phase is markedly slowed down in the dehydration scans. These hystereses are proved to be reproducible. They can be interpreted as an inherent property of the system. The time needed for the formation of crystalline phases ranges from 5 to 10 h (DODPC) to lasting several days (subgel phase of DPPC).

G. Chemical Potential of Water and Hydration Pressure

The water activity in the sample chamber, $a_w \equiv \mathrm{RH}/100\%$, is directly related to the difference of the chemical potential of water at $a_w < 0$ and bulk water ($a_w(\mathrm{bulk}) = 1$)

$$\Delta\mu_W \equiv \mu_W(a_W < 1) - \mu_W(a_W = 1) = \mathrm{RT} \cdot \ln a_W \tag{2.1}$$

(R is the gas constant). Hydrated amphiphiles represents a two component mixture. One can formally write $a_w = \gamma_W \cdot x_W$ where γ_W and $x_{W/L} = R_{W/L}/(R_{W/L} + 1)$ denote the activity coefficient and the mole fraction of water in the sample, respectively. Rearrangement provides a simple form of the adsorption isotherm

$$R_{W/L}(a_W) = a_W/(\gamma_W - a_W) \tag{2.2}$$

The isotherm referring to the ideal mixing of the components ($\gamma_W = 1$) has been marked by dotted lines in the $R_{W/L}$ plots shown in Fig. 3. Real and ideal isotherms reveal markedly different courses. The considerable difference in molecular volume between water and lipid and, first of all, specific interactions between the components (especially at RH < 80%) give rise to highly nonideal properties of the mixtures.

The so-called isotropic hydration pressure,[26]

$$\Pi \equiv -\frac{\Delta\mu_W}{v_W}, \tag{2.3}$$

represents a sort of (negative) osmotic stress, which compresses the sample upon dehydration. It corresponds to the pressure, which should be applied to dehydrate the system down to $R_{W/L}$. The partial molar volume of water in the mixture, v_W, can be set equal to the molar volume of pure water ($1.8 \cdot 10^{-5}\,m^3/mol$) at $\Pi < K_W$ where $K_W \approx 200$ GPa is the compressibility modulus water.

H. Lyotropic Phase Behaviour

Dehydration can be interpreted in terms of increasing hydration pressure according to Eq. (2.3). Consequently, lyotropic and barotropic phase transitions are based on similar molecular effects. The removal of water from the polar part of amphiphiles decreases the mean distance between neighbouring molecules. As a consequence the intermolecular forces increase. This tendency can induce conformational changes such as the straightening of the lipid acyl chains at the liquid crystalline-to-gel phase transition. Such lyotropic chain freezing transitions could be easily detected by the sigmoidal shift of the methylene stretching frequency (cf Fig. 4).

The humidity titration technique allows to perform hydration/dehydration scans at different temperatures. The position of the chain melting transition of POPC and DMPC shifts to smaller RH values upon heating (Fig. 4). The phase transition data were collected into a $T - \Delta\mu_W/\Pi$ plot (Fig. 5). The gel/liquid crystalline phase boundaries of disaturated DMPC and of monounsaturated POPC are offset one to another, but both lines run almost parallel. Their mean slope of 0.15–0.20 K/MPa agrees with the slope of the respective phase transition lines of barotropic T–p phase diagrams (22 K/MPa).[21] This result clearly illustrates the similar character of barotropic and lyotropic experiments on lipid assemblies.

MARCEL DEKKER, INC. • 270 MADISON AVENUE • NEW YORK, NY 10016

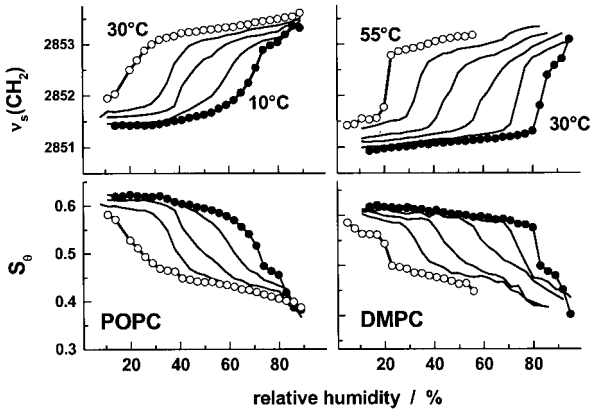

Figure 4. Center of gravity of the symmetric methylene stretching band (above) and chain order parameter (below) of POPC (left) and DMPC (right) as a fuction of RH. The graphs refer to different temperatures. The increment of temperature between the hydration scans was +5 K (from right to left).

A modified Clausius–layperon equation relates the slope of the transition line in the $\Delta\mu_W - T$ diagram to the alteration of the partial molar entropy of water, $s_W \equiv \partial S/\partial R_{W/L}$, at the transition.[30,38,39]

$$\frac{d\Delta\mu_W}{dT} = -\Delta s_W. \tag{2.4}$$

The chain melting is accompanied by a considerably gain of entropy ($\Delta s_W > 0$) owing to the higher degree of conformational disorder of the chains in the fluid phase. Equation (2.4) predicts a negative slope for this entropy-driven event, which is actually observed for the respective transition lines (Fig. 5).

Another type of phase transformation, the so-called solvation induced transition, possesses a positive slope for a lipid with PC headgroups (DODPC) and a negative slope for a lipid with PE headgroups (DOPE) (cf Fig. 6).[30] Consequently, the solvation-induced transition of DOPE shows to be entropy-driven ($\Delta s_W > 0$), and that of DODPC is enthalpy-driven ($\Delta s_W < 0$). This difference was rationalised in terms of direct hydrogen bond formation between the PE headgroups and its absence for PC headgroups.[3,30] The PC headgroups gain enthalpy upon solvation because they form H-bonds to the water. Contrarily, PE–PE hydrogen bonds were partially substituted by water–PE hydrogen bonds of similar enthalpy. The increase of molecular

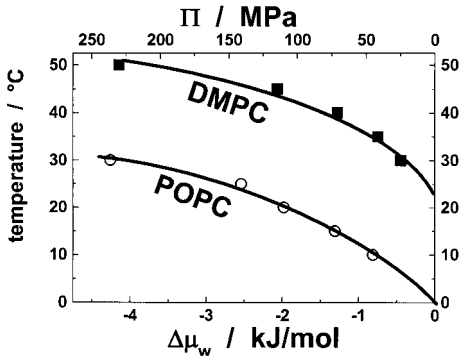

Figure 5. Gel/fluid phase transition temperatue of POPC and DMPC as a function of the chemical potential of water (abscissa below, Eq. (2.1)) and hydration pressure (abscissa above, Eq. (2.3)). The symbols refer to the midpoints of the sigmoidal change of COG($\nu_s(CH_2)$) shown in Fig. 4.

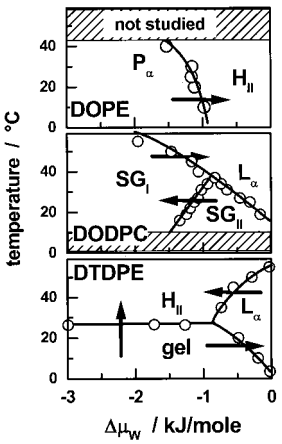

Figure 6. Lyotropic phase diagrams of lipids: dioleoyl PC (DOPE), dioctadecadienoyl PC (DODPC) and ditetradecadienoyl PC (DTDPC). Open circles denote experimental transition data. The phases are the ribbon phase (P_α), the inverse hexagonal phase (H_{II}), two subgel phase differing in headgroup structure (SG_I and SG_{II}), the liquid crystalline phase (L_α), and the gel phase. See refs.[2,3] for details. The arrows point in direction of increasing entropy across the phase transitions. Solvation-induced headgroup transitions of DOPE and DTDPE take place between the P_α and H_{II} and between the SG_I and SG_{II} phases, respectively.

MARCEL DEKKER, INC. • 270 MADISON AVENUE • NEW YORK, NY 10016

disorder in the headgroup region of DOPE finally causes the gain of entropy and the negative slope of the transition line.

Also other types of enthalpy-driven lyotropic phase transitions have been detected by hydration-tuning infrared studies[2,33] (vide infra). Water binding to lipids can induce the transition between the inverse hexagonal (H_{II}) and the lamellar liquid crystalline (L_α) phase (Fig. 6)[2] or the transition between the so-called expanded liquid crystalline (L_α') and the "usual" L_α phase.[33,39] At the H_{II}/L_α transition, curved lipid layers unbend to flatness, whereas fluid bilayers contract in lateral direction at the L_α'/L_α transition. The conformational order of the acyl chains increases in both cases.

Subtle alterations of headgroup orientation, chain ordering and aggregate morphology could be detected by linear dichroism measurements at these phase transitions (vide infra). Note that the respective shift of the average CH_2 stretching frequency is rather small because the acyl chains remain in the fluid, or in the all-trans state before and after the transition (cf Fig. 3, DOPE and DTDPC, respectively).

I. Oriented Films

Many amphiphilic aggregates spontaneously align on solid surfaces forming macroscopically oriented molecular structures. This property enables preparation of oriented lipid multibilayer stacks by spreading appropriate amounts of an organic stock solution of the lipid on the surface of the ATR crystal. Volatile solvents, such as methanol or methanol/chloroform mixtures, are evaporating in minutes leaving oriented cast films. Also the drying of droplets of aqueous vesicle suspensions (multilamellar or unilamellar vesicles) under a stream of warm air or nitrogen was found to provide highly oriented films.

The average thickness of such cast films is found in the order of a few micrometers. It corresponds to a stack of about 500–2000 bilayers. The underlying solid support only influences the phase behaviour and local molecular ordering of a few bilayers, which are in direct contact with the surface. The properties of more distant bilayers remain virtually unaffected.[40,41] Consequently, oriented cast films allow to investigate bulk material properties.

The absorption of linearly polarised light by oriented films in general depends on the polarisation direction. This property is called linear dichroism. Spectroscopically, it reveals molecular ordering. Linear dichroism combined with infrared spectroscopy is a powerful tool to study the architecture of amphiphilic aggregates on a molecular level

MARCEL DEKKER, INC. • 270 MADISON AVENUE • NEW YORK, NY 10016

because the spectral information about molecular conformations and interactions is supplemented by information about molecular orientation. The basic formulae to analyse the results of IR linear dichroism measurements in terms of molecular ordering are introduced and discussed in the following section.

III. INFRARED ABSORPTION AND MOLECULAR ORDER

J. Absorption of Polarised Light

Infrared spectroscopy is based on the absorption of electromagnetic radiation by matter due to the interaction of the electric field with oscillating permanent dipoles (so-called transition dipoles), which are provided by vibrational modes of chemical bonds. A vibrational mode is characterised by its frequency (wavelength or wavenumber) and the absorption "strength" defined by the absorbance, $A = -\log_{10}(I/I_0)$ where I_0 and I denote the intensity of the light before and after absorption, respectively. On a microscopical level, the absorbance of polarised electromagnetic radiation is given by the ensemble average of the squared scalar product of the unit vectors, $\boldsymbol{\mu}$ and $\mathbf{e}$ pointing along the individual transition dipoles of the IR active groups and the electric field vector, respectively (see Fig. 7),

$$A = A_{\max} \frac{\left\langle \varepsilon \cdot (\mu \cdot \mathbf{e})^2 \right\rangle}{\langle \varepsilon \rangle}. \tag{3.1}$$

$A_{\max}$ is the maximum absorbance corresponding to a sample with transition dipoles, which perfectly align parallel to $\mathbf{e}$. The respective molar extinction coefficient, ε (defined as the absorbance of one mole of absorbing groups), represents a microscopic property, which in general depends on the conformation and/or local environment of the IR-active group. Therefore, it has been included into the ensemble average, $< \cdots >$. It is useful to decompose the absorbance, A, into two parts. The first one corresponds to the isotropic sample, $A_{\text{iso}} = A_{\max}/3$, whereas the second one refers to the anisotropic contribution due to molecular orientations, δA,

$$A = \tfrac{1}{3} A_{\max} + \delta A. \tag{3.2}$$

The latter term can be written in the form[1]

$$\delta A = \tfrac{2}{3} A_{\max} \cdot S_{\text{IR}} \cdot P_2(\alpha') \tag{3.3}$$

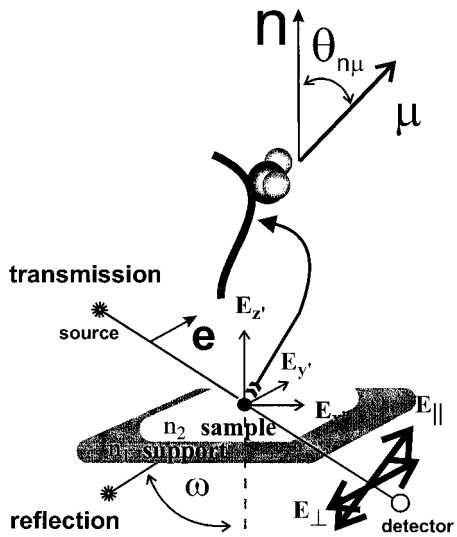

Figure 7. Geometry of the IR absorption experiment. The sample is spread on a solid support, which is transparent in the mid IR region. In the transmission experiment the support is given by a window, in the reflection experiment by the ATR crystal. $E_{x'}$, $E_{y'}$ and $E_{z'}$ denote the projections of the polarised electric field amplitude, **e**, in the laboratory $\{x', y', z'\}$ frame. Polarization in parallel and perpedicular direction relative to the plane of incidence provides $E_{\parallel} = \sin\omega\ E_{x'} + \cos\omega\ E_{z'}$ and $E_{\perp} = E_{y'}$. **μ** and **n** denote unit vectors pointing along the normal of the support and along the transition moment of the IR active group. Both vectors enclose the angle $\theta_{n\mu}$.

where S_{IR} represents the so-called infrared (or optical) order parameter

$$S_{\mathrm{IR}} \equiv \frac{\langle \varepsilon \cdot P_2(\theta_{\mu n}) \rangle}{\langle \varepsilon \rangle} \qquad \text{with } P_2(\theta_{\mu n}) \equiv \tfrac{1}{2}(3 \cdot (\mu \cdot n)^2 - 1). \tag{3.4}$$

$P_2(x) \equiv 0.5(3\cos^2 x - 1)$ denotes the second-order Legendre polynomial. The angle $\theta_{\mu n}$ is enclosed between the transition moment and the normal of the surface of the optical element, **n**, which supports the sample (e.g., a window or the ATR crystal). The polarisation direction and **n** enclose the angle α'. Consequently, the absorbance of light, which is polarised along one of the axes of a cartesian $\{x', y', z'\}$-system (z' points parallel to **n**), can be obtained after making use of Eqs. (3.2) and (3.3) with $\alpha' = 0^\circ$

and 90°, respectively,

$$\begin{aligned} A_{z'} &= A_{\max} \cdot (1 + 2 \cdot S_{IR}) \quad \text{and} \\ A_{x'} &= A_{y'} = A_{\max} \cdot (1 - S_{IR}). \end{aligned} \tag{3.5}$$

Typically, light of electric field strength E_0 enters the sample in an oblique fashion. Let us define the plane of incidence by the coordinate axes x' and z'. The absorbance for polarisation directions, parallel and perpendicular with respect to the plane of incidence depends on $A_{x'}$, $A_{y'}$ and $A_{z'}$ and the respective projections of the electric field amplitudes on the coordinate axes, $E_{x'}$, $E_{y'}$ and $E_{z'}$ (see Fig. 7),

$$\begin{aligned} A_{\parallel} &= \left(\frac{E_{x'}}{E_0}\right)^2 \cdot A_{x'} + \left(\frac{E_{z'}}{E_0}\right)^2 \cdot A_{z'} \quad \text{and} \\ A_{\perp} &= \left(\frac{E_{y'}}{E_0}\right)^2 \cdot A_{y'}. \end{aligned} \tag{3.6}$$

Combination of Eqs. (3.5) and (3.6) provides

$$\begin{aligned} A_{\parallel} &= k \cdot (K_1 + K_2 \cdot S_{IR}) \quad \text{and} \\ A_{\perp} &= k \cdot (1 - S_{IR}) \end{aligned}$$

with

$$K_1 = \frac{E_{z'}^2 + E_{x'}^2}{E_{y'}^2}, \qquad K_2 = \frac{2E_{z'}^2 - E_{x'}^2}{E_{y'}^2}$$

$$\text{and} \quad k = A_{\max} \cdot \left(\frac{E_{y'}}{E_0}\right)^2. \tag{3.7}$$

According to Eq. (3.7) the absorbance of linearly polarised light changes with the polarisation direction if the absorbing dipoles are ordered with respect to the optical axis ($S_{IR} \neq 0$). This phenomenon is called linear dichroism. Let us introduce the dichroic ratio

$$R \equiv \frac{A_{\parallel}}{A_{\perp}} = \frac{K_1 + K_2 \cdot S_{IR}}{1 - S_{IR}} \tag{3.8}$$

as the essential experimental parameter, which characterises the linear dichroism of a sample. Two additional combinations of the polarised absorbances $A_{\parallel}$ and $A_{\perp}$ are of interest:

$$\begin{aligned} \Delta A &\equiv A_{\parallel} - K_1 \cdot A_{\perp} = k \cdot (K_2 - K_1) \cdot S_{IR} \quad \text{and} \\ \Sigma A &\equiv A_{\parallel} + K_2 \cdot A_{\perp} = k \cdot (K_1 + K_2). \end{aligned} \tag{3.9}$$

The weighted difference, ΔA, is directly related to S_{IR}. Note that the proportionality constant k is proportional to A_{max} (cf Eq. (3.7)), which depends on the mean extinction coefficient and on the number of absorbing groups in the sample ($A_{max} \propto n_{group} \cdot <\varepsilon>$). Hence, the difference ΔA (also called linear dichroism) is a function of the molecular order, of n_{group} and of the optical property $<\varepsilon>$. Different ΔA values of two particular absorption bands do not necessarily reflect different mean orientations of the respective IR active groups. The dichroic ratio provides however a clear criterium of the molecular order because the optical parameters K_1 and K_2 are constants for a chosen experimental set-up if one neglects the dispersion of the refractive index (see next paragraph).

The weighted sum, ΣA, does not depend on S_{IR}, and thus it is independent of the molecular order in the sample. Consequently, $A = \Sigma A$ provides the absorbance of the respective isotropic (macroscopically disordered) sample. Optical parameters, such as the maximum position, the centre of gravity and the integral absorbance of an absorption band, must be extracted from the weighted sum spectrum, ΣA, to avoid interference with molecular ordering. Note, that the ATR experiment yields $A = k\{(K_1 + 1) + S_{IR}((K_2 - 1)\}$ if non-polarised IR radiation is used. In this case, the absorbance depends on the degree of macroscopic molecular ordering.

K. Measurement of IR Order Parameters: Transmission and Attenuated Total Reflection

Rearrangement of Eq. (3.8) provides the infrared order parameter as a function of the dichroic ratio and of the constants K_1 and K_2

$$S_{IR} = \frac{R - K_1}{R + K_2}. \tag{3.10}$$

According to this result, the order parameter of an IR active group can be determined by using light, which is being polarised in parallel and perpendicular direction with respect to the plane of incidence. The optical constants K_1 and K_2 are functions of the components of the electric field in the sample (cf Eq. (3.7)), which in turn depend on the angle of incidence, ω, on the refractive indices of the involved media (solid support, sample and partly the medium "above" the sample, usually air or water, n_1, n_2 and n_3, respectively) and on the type of the experiment (see below).

MARCEL DEKKER, INC. • 270 MADISON AVENUE • NEW YORK, NY 10016

In the transmission experiment the infrared light passes both through the sample and the IR transparent window, which supports the film. In the attenuated total reflection experiment the IR beam is reflected within an internal reflection element (ATR crystal). Here, an evaniscent IR wave is set up into the sample that is supported by the reflecting surface. The penetration of the electromagnetic field into the optical rarer medium enables its characterisation by absorption spectroscopy.

Application of Fresnels equations in the limit of weak absorption provides the electric field amplitudes, and thus the optical constants for the transmission and attenuated total reflection (ATR) experiments (cf Ref.[9,42] for details):

Transmission

$$\begin{bmatrix} E_{x'}^2 \\ E_{y'}^2 \\ E_{z'}^2 \end{bmatrix}_{\text{transmission}} = \begin{bmatrix} 1 - \frac{\sin^2\omega}{n_{23}^2} \\ 1 \\ \frac{\sin^2\omega}{n_{23}^2} \end{bmatrix} \cdot E_0^2$$

$$K_1 = 1 \quad \text{and} \quad K_2 = 3 \cdot \frac{\sin^2\omega}{n_{23}^2} - 1 \tag{3.11}$$

Attenuated Total Reflection (Approximation of Thick Layer, $d >> d_p$)

$$\begin{bmatrix} E_{x'}^2 \\ E_{y'}^2 \\ E_{z'}^2 \end{bmatrix}_{\text{ATR}}^{\text{thick layer}} = \begin{bmatrix} \frac{\sin^2\omega - n_{21}^2}{(1+n_{21}^2)\cdot\sin^2\omega - n_{21}^2} \\ 1 \\ \frac{\sin^2\omega}{(1+n_{21}^2)\cdot\sin^2\omega - n_{21}^2} \end{bmatrix} \cdot \frac{4\cos^2\omega \cdot E_0^2}{(1-n_{21}^2)}$$

$$K_1 = \frac{2\cdot\sin^2\omega - n_{21}^2}{(1+n_{21}^2)\cdot\sin^2\omega - n_{21}^2} \quad \text{and}$$

$$K_2 = \frac{\sin^2\omega + n_{21}^2}{(1+n_1^2)\cdot\sin^2\omega - n_{21}^2} \tag{3.12}$$

MARCEL DEKKER, INC. • 270 MADISON AVENUE • NEW YORK, NY 10016

Attenuated Total Reflection (Approximation of Thin Layer, $d << d_p$)

$$\begin{bmatrix} E_{x'}^2 \\ E_{y'}^2 \\ E_{z'}^2 \end{bmatrix}_{\text{ATR}}^{\text{thin layer}} = \begin{bmatrix} \dfrac{\sin^2\omega - n_{31}^2}{(1+n_{31}^2)\cdot\sin^2\omega - n_{31}^2} \\ 1 \\ \dfrac{\sin^2\omega \cdot n_{32}^2}{(1+n_{31}^2)\cdot\sin^2\omega - n_{31}^2} \end{bmatrix} \cdot \frac{4\cos^2\omega \cdot E_0^2}{(1-n_{31}^2)}$$

$$K_1 = \frac{(1+n_{32}^2)\cdot\sin^2\omega - n_{31}^2}{(1+n_{31}^2)\cdot\sin^2\omega - n_{31}^2} \quad \text{and}$$

$$K_2 = \frac{(2n_{31}^2 - 1)\cdot\sin^2\omega + n_{31}^2}{(1+n_{31}^2)\cdot\sin^2\omega - n_{31}^2} \tag{3.13}$$

Figure 8 illustrates the relation between the dichroic ratio and the IR order parameter for selected set-ups. The thick film ATR experiment (cf next paragraph) ensures the best sensitivity of the observable R in the most relevant range of IR order parameters, $-0.5 \leq S_{\text{IR}} < 0.5$ (cf below). Table 1 lists values of the optical constants for ATR and transmission experiments.

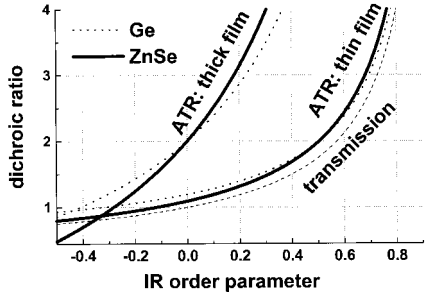

Figure 8. Dichroic ratio, R, as a function of the IR order parameter. R has been calculated by means of Eq. (3.10) for the special cases of the transmission (Eq. (3.11) and ATR (thick and thin film, Eqs. (3.12) and (3.13)) experiments. The angle of incidence is $\omega = 45°$. The refractive indices correspond to lipid (sample, $n_2 = 1.42$), air ($n_3 = 1$) and Ge or ZnSe ATR crystals ($n_1 = 4.0$ and 2.44, respectively).

Table 1. Optical constants.[a]

ATR material	ZnSe		Ge	
Refractive index	2.44		4.0	
Penetration depth[b]	1.6–2.3 μm		1.1–1.5 μm	
Constants	K_1	K_2	K_1	K_2
Thick film	2.0	2.54	2.0	1.43
Thin film ($n_3 = 1.0$)[c]	1.09	−0.21	1.20	−0.41
Thin film ($n_3 = 1.33$)[c]	0.93	0.12	1.15	−0.32
Transmission[d]	1.0	−0.52		

[a]Angle of incidence, $\omega = 45°$; refractive index of the sample, $n_2 = 1.42$; K_1 and K_2 are calculated by means of Eqs. (3.11), (3.12) and (3.13).
[b]The range corresponds to the mid infrared (wavelengths $\lambda = 0.25$–$1.5\,\mu m$ and wavenumbers 4000–700 cm^{-1}).
[c]$n_3 = 1.0$ and 1.33 correspond to air and water, respectively.
[d]The optical constants are independent of the window material in the transmission experiment.

L. Penetration Depth and Sample Thickness

The ATR experiment is a surface sensitive technique, which probes a thin layer not exceeding a thickness of a few micrometer adjacent to the surface of the ATR crystal (see below). The major advantages of this method are the greatly reduced absorption of bulk media, such as water, and the fact that the molecules can be fairly well oriented near the surface. "Thick" films are of macroscopic thickness compared with the molecular dimensions, so that one virtually probes a bulk system whose properties are only weakly affected by the solid support.

The nominal penetration depth of the electromagnetic field into the sample

$$d_p = \frac{\lambda}{2\pi \cdot n_1 \cdot \sqrt{(\sin^2 \omega - n_{21}^2)}} \tag{3.14}$$

characterises the optical thickness of the absorbing layer (cf Table 1).

The dichroic ratio of a particular sample strongly depends on its real thickness, d, because the electromagnetic field, and thus also the optical constants K_1 and K_2 are functions of d (cf Fig. 9). On principle,

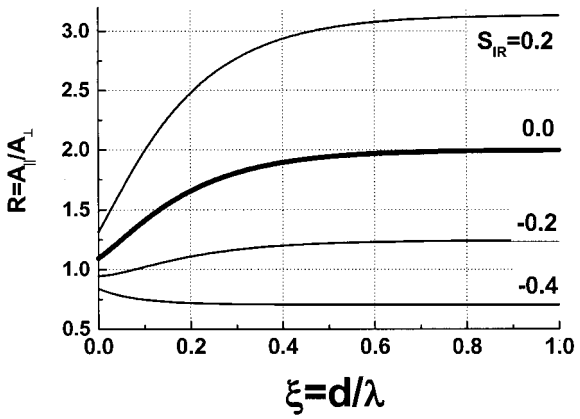

Figure 9. Dichroic ratio corresponding to different IR order parameters as a function of the mean relative thickness of the sample film on the ATR crystal, $\xi = d/\lambda$, where d and λ denote the mean thickness of the film and the wavelength, respectively. For details of the calculation see Ref.[1]

the interpretation of the dichroic ratio in terms of S_{IR} requires the knowledge of the film thickness or, alternatively, the realisation of the limiting cases of "thin" or "thick" films. To estimate the potential error for films of intermediate thickness, we calculated the "apparent" IR order parameter, S_{IR}^{thick}, by means of the thick film approximation for films whose real thickness does not exactly match the condition $d >> d_p$ (Fig. 10). This study is proof that the thick film approximation guarantees good results for $d/\lambda > 0.2$ (λ is the wavelength of absorbed light). The "apparent" order parameter potentially underestimates the real one at $S_{IR}^{thick} > -0.25$.

Note that the preparation of "thick" films for lyotropic experiments (vide supra) is relatively simple, and that it usually ensures intense spectra. In practice it is convenient to spread the available amount of material over an area that guarantees a sufficient film thickness even if the film only partly covers the full length of the ATR surface.

M. Birefringence and Inner Field

The linear dichroism reflects the degree of anisotropy of molecular orientations in the sample. Also other optical properties, such as the

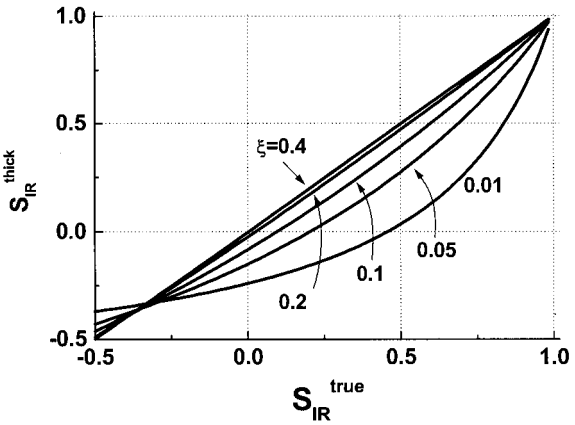

Figure 10. Correlation plot between the apparent IR order parameter, $S_{\mathrm{IR}}^{\mathrm{thick}}$, calculated by means of the thick film approximation and its true value, $S_{\mathrm{IR}}^{\mathrm{true}}$, for sample films of different thickness. The relative thickness, $\xi \equiv d/\lambda$, increases from $\xi = 0.01$ to 0.4. The deviation from the diagonal line ($S_{\mathrm{IR}}^{\mathrm{thick}} = S_{\mathrm{IR}}^{\mathrm{true}}$) illustrates the error one makes if applying the thick film approximation to thinner fims. For details of the calculation see Ref.[1]

polarisability and the refractive index are functions of the relative orientation between the symmetry axes of molecular order and the electromagnetic field. The refractive index consequently depends on the experimental setup and on the molecular ordering in analogy with the absorbance. There are two refractive indices, which are relevant in the special case of uniaxial systems: the first one for the ordinary (n_2^o) and the second one for the extraordinary (n_2^{ao}) beam with electrical field vectors pointing perpendicular and parallel to the director (see below). For oblique incidence one has to consider the weighted mean, $n_2^{\omega} = n_2^o \cdot (1 - \sin^2 \omega \cdot (n_2^{\mathrm{ao}^{-2}} - n_2^{o^{-2}}))^{1/2}$.[43]

In addition, the anisotropic character of the absorbing medium distorts the local electric field.[44] This so-called inner field effect can be taken into account by means of the correction factor $g \equiv (n_2^{\mathrm{ao}}/n_2^o) \cdot (f^{\mathrm{ao}}/f^o)$, which scales the z'-component of the electric field in Eq. (3.7), $E_{z'} \rightarrow g \cdot E_{z'}$. The field factors of the ordinary and extraordinary beam, f^o and f^{ao}, are functions of the respective refractive indices and of the shape of the absorbing molecule.[44]

A theoretical analysis showed that neglecting birefringence and inner field in the data analysis can give rise to small systematic errors, which, typically, tend to overestimate molecular order.[1] The anomalous

MARCEL DEKKER, INC. • 270 MADISON AVENUE • NEW YORK, NY 10016

dispersion of the ordinary and extraordinary refractive indices partly explains the dispersion-like variation of the wavenumber-dependent dichroic ratio, which is observed with most of the absorption bands (see below and Ref.[40]).

N. Molecular Order

The most important question in structural studies arises about the orientation and/or conformation of molecules in a particular structure. The infrared order parameter provides a measure of the mean orientation of the respective transition moment, **μ**, with respect to the normal of the solid support, **n** (cf Eq. (3.4)). Consequently, it is necessary to define the orientation of **μ** within the vibrating atomic group and to extract its mean orientation from the IR linear dichroism data. In a first step, we will treat the molecular order within a supramolecular structure, which is characterised by the local director, **d**. It is defined by the unit vector, which points normal with respect to the surface in planar or curved monolayer related structures. In the second step we will handle the shape of the aggregates and their alignment on the solid support (see next paragraph).

Let us introduce two cartesian coordinate systems. The first one, $\{x, y, z\}$, is fixed to the respective atomic group (cf Fig. 11 for illustration). The orientation of the transition moment, **μ** within $\{x, y, z\}$ is defined by the polar angles α and β. The z_d-axis of the second system, $\{x_d, y_d, z_d\}$, points along the director **d**. The orientation of the molecular system within the considered layer is defined by the tilt θ (the angle between z and z_d) and the azimuth ψ (the angle of rotation about z in counter-clockwise direction).

It has been shown that the second order Legendre polynomial of the angle between **μ** and **d**,

$$S_\mu \equiv \langle P_2(\theta_{\mu d})\rangle = \tfrac{1}{2}\langle 3\cdot(d\cdot\mu)^2 - 1\rangle, \tag{3.15}$$

can be decomposed into a sum of molecular order parameters, which are functions of the molecular orientation defined by θ and ψ and of prefactors, which are functions of the intramolecular coordinates α and β[1,45]:

$$\begin{aligned} S_\mu = {} & S_\alpha \cdot S_\theta + \tfrac{1}{3}\left(D_{\alpha\beta}\cdot D_{\theta\psi} - C_{\alpha\beta}\cdot C_{\theta\psi}\right) \\ & - \tfrac{1}{3}\left(D'_{\alpha\beta}\cdot D'_{\theta\psi} + C'_{\alpha\beta}\cdot C'_{\theta\psi}\right) \end{aligned} \tag{3.16}$$

MARCEL DEKKER, INC. • 270 MADISON AVENUE • NEW YORK, NY 10016

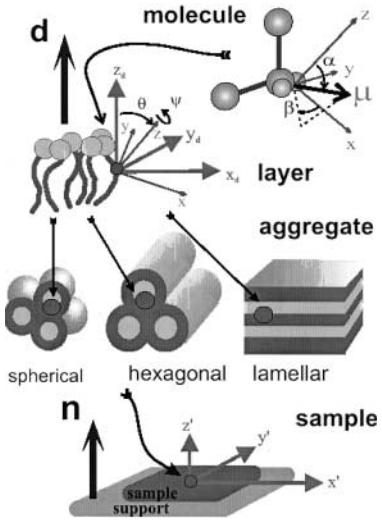

Figure 11. Hierarchy of molecular order in cast films of hydrated amphiphiles used in IR spectroscopy. From top to bottom: Cartesian $\{x, y, z\}$ system fixed to the vibrating IR active atomic group (e.g., a methylene group). The polar angles α and β define the orientation of the transition moment $\boldsymbol{\mu}$. The molecules (e.g., lipids) assemble into monolayer-related structures, which are characterised by the director, **d**. $\{x_d, y_d, z_d\}$ is a cartesian system with z_d pointing along **d**. The angles θ and ψ provide the tilt and azimuth of the $\{x, y, z\}$ frame with respect to the $\{x_d, y_d, z_d\}$ system. The monolayers form superstructures of spherical, hexagonal or lamellar morphology. The laboratory frame, $\{x', y', z'\}$, defines the plane of incidence (x'–z') and the normal of the solid support, z' (see also Fig. 7).

with the definitions

$$
\begin{aligned}
S_a &= \tfrac{1}{2}\left(3 \cdot \langle \cos^2 a \rangle - 1\right) \\
D_{ab} &= \tfrac{3}{2}\langle \sin^2 a \cdot \cos 2b \rangle; \qquad D'_{ab} = \tfrac{3}{2}\langle \sin^2 a \cdot \sin 2b \rangle \\
C_{ab} &= \tfrac{3}{2}\langle \sin 2a \cdot \cos b \rangle; \qquad C'_{ab} = \tfrac{3}{2}\langle \sin 2a \cdot \sin b \rangle \\
&\text{with} \quad a, b = \alpha, \beta \quad \text{and} \quad \theta, \psi
\end{aligned} \tag{3.17}
$$

Here we assume that the probability distribution of the tilt for rotations about z_d be of cylindrical symmetry. Eq.(3.16), further, assumes that the orientation of the transition moment within the molecular frame is fixed, and independent of the molecular orientation given within the $\{x_d, y_d, z_d\}$ frame of the layer. It is important to note that this treatment includes the possibility of biaxiality, which is characterised by longitudinal (tilt) and transverse (azimuth) molecular order.

MARCEL DEKKER, INC. • 270 MADISON AVENUE • NEW YORK, NY 10016

O. Macroscopical Order and Aggregate Morphology

Amphiphilic molecules, typically, form aggregates, which arrange into superstructures. Hydrated lipids in many cases spontaneously assemble into multibilayer-water stacks. Their interfacial planes predominantly orient parallel to the solid support. Nonlamellar phases of spherical (e.g., micelles) or cylindrical (e.g., hexagonal or inverse - hexagonal phases) aggregates can form at certain conditions. Molecules also orient spontaneously when incorporated within a host matrix. Liquid crystals and detergents arrange at the inner surface of confining geometries such as nanopores[43] or layered minerals.[46] A second example are peptides and proteins, which orient upon insertion into lipid membranes.

To consider such superstructures we define the order parameter of aggregate morphology as the mean second order Legendre polynomial of the angle between the local director **d** and the optical axis, **n**

$$S_d \equiv \langle P_2(\theta_{dn}) \rangle = \tfrac{1}{2}\langle 3 \cdot (n \cdot d)^2 - 1 \rangle. \tag{3.18}$$

Averaging refers to all orientations of the local director within the sample. Note that Eq. (3.18) assumes cylindrical symmetry of the distribution of **d** about **n**. This condition is rational in most cases because the sample films possess macroscopic dimensions in parallel direction to the solid support. For the special cases of (i) ideally flat membranes, which align parallel to the ATR surface, (ii) cylinders with their axes parallel and (iii) perpendicularly to the ATR surface, and (iv) spheres, one obtains $S_d^{\text{mem}} = 1$ (i), $S_d^{\text{cyl}} = 0.25$ (ii), $S_d^{\text{cyl},\perp} = -0.5$ (iii) and $S_d^{\text{sph}} = 0$ (iv) after averaging.[2,3]

In addition, one has to consider that the surface of the aggregates is not perfectly smooth owing to undulations and protrusions of the molecules. Furthermore, the aggregates do not perfectly align on the solid support in the assumed fashion. These effects decrease the absolute value of S_d by a factor $0 \leq S_o < 1$, which is defined as the mean second order Legendre polynomial of the fluctuation angle of the local director.

P. IR Order Parameter

In the last two paragraphs we defined two order parameters. The latter one, S_d, considers the degree of macroscopic ordering and/or the aggregate morphology whereas S_μ quantifies the order of the molecules

MARCEL DEKKER, INC. • 270 MADISON AVENUE • NEW YORK, NY 10016

within the aggregates. The IR order parameter can be expressed as the product:

$$S_{\mathrm{IR}} = S_d \cdot S_\mu. \tag{3.19}$$

If the macroscopic ordering possesses cylindrical symmetry with respect to the optical axis **n,** and if the relative orientations of **n**, **d** and **μ** are independent of each other. Equation (3.19) provides the output of the IR linear dichroism experiment (cf Eq. (3.10)) as a function of the molecular order in the aggregates (cf Eq. (3.16)) and as a function of their macroscopic alignment in the cast film (cf Eq. (3.18)).

According to Eq. (3.19), linear dichroism measurements are expected to detect alterations of aggregate morphology with high sensitivity. Especially transitions between lamellar and nonlamellar phases should be characterised by marked changes of IR order parameters because of the drastic drop of S_d from unity to values less than 0.25.

Q. Mean Orientation

It seems useful to interpret the IR order parameter in terms of the mean tilt angle, $\theta_{d\mu}$, of the transition moment, **μ**, with respect to director, **d**,

$$< \theta_{\mu d} > \approx \arccos\left(\sqrt{\tfrac{1}{3} \cdot \left(2\frac{S_{\mathrm{IR}}}{S_d} + 1\right)}\right). \tag{3.20}$$

It provides an impression of the mean orientation of **μ** in the molecular aggregates. This transformation only yields adequate results if the distribution of the tilt is limited to a relatively narrow angular range, and if the degree of macroscopic ordering is known or nearly perfect. In many situations one assumes $S_d = 1$, and thus overestimates the real ordering. Then Eq. (3.20) provides mean tilt angles, which are systematically shifted towards the magic angle (54°).

IV. THE MOLECULAR ARCHITECTURE OF LIPID MEMBRANES AS SEEN BY IR LINEAR DICHROISM SPECTROSCOPY

R. IR Active Modes and Linear Dichroism of Lipids

Figure 12 displays typical polarised spectra of a lipid (POPC), which is spread as a cast film on the surface of the ATR crystral (ZnSe).

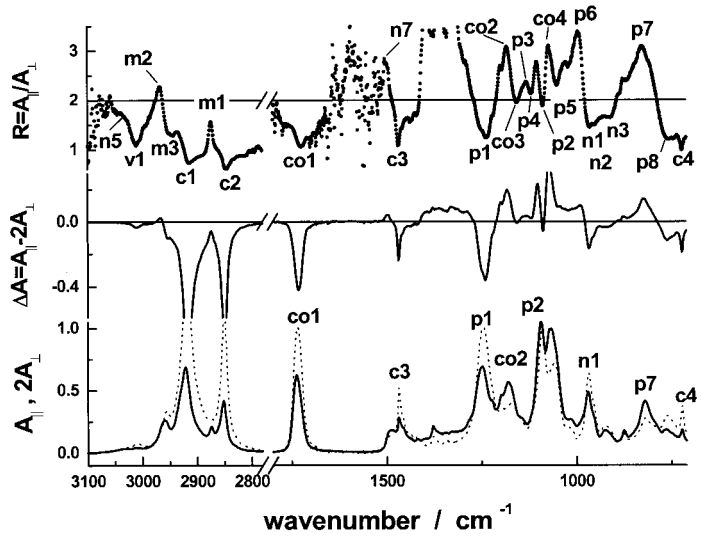

Figure 12. Polarised ATR-IR absorption spectra, $A_{\parallel}(\nu)$ and $2A_{\perp}(\nu)$ (below), difference spectrum, $\Delta A\ (\nu) = A_{\parallel}(\nu) - 2A_{\perp}(\nu)$ (middle), and spectrum of the dichroic ratio, $R(\nu) = A_{\parallel}(\nu)/A_{\perp}(\nu)$ (above), of POPC in the gel state (RH = 10%, $T = 25^{\circ}$C). Selected bands are assigned according to Table 2. See also Fig. 13 to compare the orientation of the transition moments with the observed dichroism.

The pronounced difference between $A_{\parallel}(\nu)$ and $2A_{\perp}(\nu)$ reveals strong linear dichroism of most of the absorption bands. The interpretation of the dichroic ratio of a selected absorption band in terms of molecular order requires the knowledge of the orientation of the respective transition moments within the lipid molecule. Normal coordinate analyses indicate considerable vibrational mixing between different modes especially for the polar headgroups but also for the acyl chains.[47,48] Therefore the orientation of most of the transition moments within the respective chemical group is not precisely known. Nearly each of the considered atomic groups gives however rise to several absorption bands. The orientation of the respective transition moments can be deduced from the comparative analysis of the measured IR order parameters, reasonable assumptions about the respective change of charge density caused by the vibration and also from the linear dichroism of macroscopically oriented molecular assemblies in which the orientation of these groups is approximately known (for example, solid phases, crystals, etc.,).

Characteristic group vibrations of the acyl chains and of PC and PE headgroups are assigned in Table 2. Quantitative analysis of an absorption band in terms of the IR order parameter must involve baseline correction and also band separation techniques to remove "parasite" IR intensities of overlapping bands. Especially the latter effect can causes considerable systematic errors of the IR order parameter of weak absorption bands and of strongly overlapped features, for example, in the spectral region 1000–1100 cm^{-1} (see Fig. 12). Typical values of IR order parameters of the absorption bands considered in this work are given in Table 2.

Differences between the polarised spectra indicate the macroscopical orientation of the sample. The difference spectrum, $\Delta A(\nu)$, and the spectrum of the dichroic ratio, $R(\nu)$ (see Eqs. (3.8) and (3.9)), are shown above the polarised spectra in Fig. 12. Negative values of $\Delta A(\nu)$ and values of $R(\nu)$ smaller than 2.0 refer to transition moments, which on the average point more perpendicular with respect to the ATR normal ($\theta_{\mu n} > 54^\circ$, cf. Eq. (3.4)). Consequently, values of $\Delta A(\nu) > 0$ and $R(\nu) > 2$ refer to $\theta_{\mu n} < 54^\circ$, i.e., to transition moments, which are directed more parallel with respect to the ATR normal. It has been stated above that $R(\nu)$ provides an absolute measure of the mean orientation whereas the difference, $\Delta A(\nu)$, depends in addition on the respective extinction coefficient and on the number of absorbing groups (vide supra). Note, for example, the very large difference between the intensities of the $\nu_s((C–H)_2)$ (v1) and $\nu_{as}(CH_2)$ (c1) modes in the $\Delta A(\nu)$ spectrum. This effect does however not reflect different orientations but it is mainly due to the much larger number of methylene groups compared with the number of vinyl moieties. The $R(\nu)$ spectrum reveals for this particular example that both transition moments are similarly oriented.

Figure 13 schematically relates the orientation of selected transition moments to the structure of the lipid molecule. Their orientation with respect to a symmetry axis pointing along the chains is roughly compatible with the linear dichroism of the polarised spectra shown in Fig. 12. Obviously the lipid molecules macroscopically orient within multibilayer stacks, which predominantly align with the ATR surface. In this case the mean orientation of the chain axes, of the local director, **d**, and of the ATR normal, **n**, point parallel.

S. Acyl Chains: Phase Behaviour and Segmential Order

For the analysis of the segmential order of the acyl chains let us introduce cartesian $\{x^i, y^i, z^i\}$-coordinate systems, which are fixed to the

MARCEL DEKKER, INC. • 270 MADISON AVENUE • NEW YORK, NY 10016

Table 2. IR order parameter of selected IR modes of phospholipids.

No	Mode[a]	Wavenumber	S_{IR}
Phosphodiester			
p1	$\nu_{as}(PO_2^-)$	1255...1225	−0.1
p2	$\nu_s(PO_2^-)$	1085...1095	+0.1...−0.1
p3	$\nu(C^C–O(P))$	1145	0.2
p4	$\nu(C^G–O(P))$	1120	<0
p5	$\nu(P–O(C^C))$	1055	−0.2
p6	$\nu(P–O(C^G))$	985	0.4
p7	$\nu_{as}(P–(OC)_2)$	805...830	>0.1
p8	$\nu_s(P–(OC)_2)$	765	−0.2
Trimethyl ammonium			
n1	$\nu_{as}(N–C)_{ip}$	970	−0.1...−0.2
n2	$\nu_{as}(N–C)_{op}$	955	−0.2
n3	$\nu_s(N–C)_t$	925	≤0
n4	$\nu_s(N–C)_g$	875	−0.2
n5	$\nu_{as}(CH_3)_{TMA}$	3030...3020	< 0
n6	$\delta_{as}(CH_3)_{TMA}$	1480	< 0
n7	$\delta_{as}(CH_3)_{TMA}$	1495	> 0
Ammonium			
a1	$\nu_{as}(CCN)_{1013}$	1013	−0.1
a2	$\nu_{as}(CCN)$	1003	−0.35
a3	$\nu_s(CCN)$	920	−0.25
a4	$\delta_{as}(NH_3)$	1638	<0
a5	$\delta_s(NH_3)$	1530	~0
Carbonyl-ester			
co1	$\nu(C=O)$	1740...1725	−0.1...−0.2
co2	$\nu_{as}(COC)_{sn1}$	1180	+0.3
co3	$\nu_{as}(COC)_{sn2}$	1170	−0.2
co4	$\nu_s(COC)$	1075	0
Methylene			
c1	$\nu_{as}(CH_2)$	2918...2920	−0.2...−0.3
c2	$\nu_s(CH_2)$	2853...2850	−0.2...−0.3
c3	$\delta(CH_2)$	1465...1472	−0.2...−0.3
c4	$\gamma_r(CH_2)$	720...726	−0.2...−0.3
Methyl			
m1	$\nu_s(CH_3)$	2875	−0.1
m2	$\nu_{as}(CH_3)_{ip}$	2965	+0.4
m3	$\nu_{as}(CH_3)_{op}$	2955	−0.2
Vinyl			
v1	$\nu_s((C–H)_2)$	3010	<−0.1

[a]Vibrations: ν, stretching; δ, bending; γ, deformation; index: *s*, symmetric; as, antisymmetric; *r*, rocking; C^G and C^C, carbons of the glycerol and choline moieties in the $–C^G–O–PO_2^––O–C^C$-fragment, resp.; for assignments see also Ref.[10]

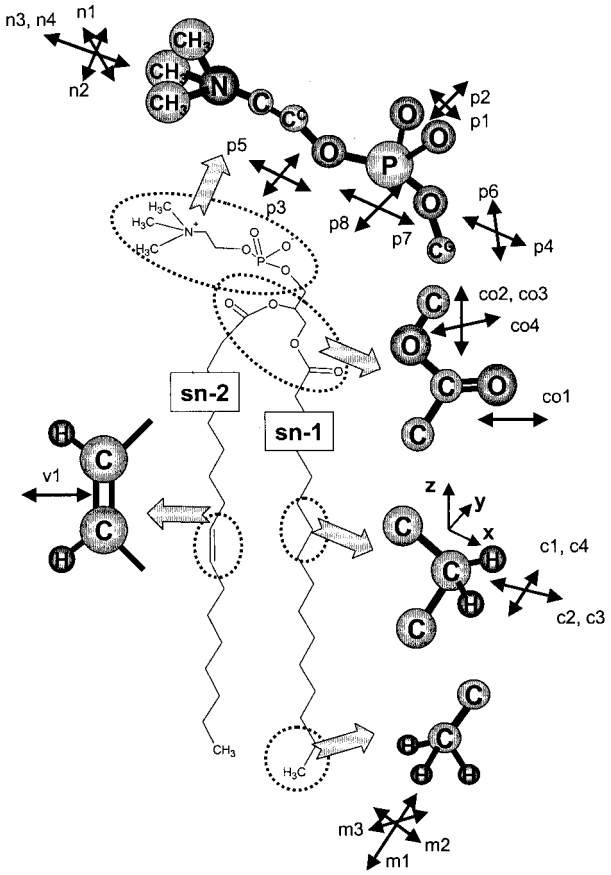

Figure 13. Transition moments of selected group vibrations of a phospholipid (POPC). The arrows schematically illustrate the orientation of the IR active transition moment **μ** within the respective atomic groups. See Table 2 for assignments.

methylene groups with axes x^i and y^i pointing along the bisector of the hydrogen–carbon–hydrogen bond angle and along the interconnecting line between both hydrogens, respectively (see Fig. 13 for illustration, the superscript i numbers the groups along the chain). The z^i-axes orient along the interconnecting line between the midpoints of adjacent C–C bonds. They define the orientation of the local fiber axis of the chain. Equation (3.16) simplifies with $(\alpha, \beta) = (90^\circ, 0^\circ)$ into $S_{\mathrm{IR}}(\nu_s(\mathrm{CH_2})) \equiv S_x = -0.5 \cdot (S_\theta - D_{\theta\psi})$ for the symmetric methylene

stretching vibration (c 2) and with $(\alpha, \beta) = (90^\circ, 90^\circ)$ into $S_{IR}(\nu_{as}(CH_2)) \equiv S_y = -0.5 \cdot (S_\theta + D_{\theta\psi})$ for the antisymmetric methylene stretching vibration (c1). Combination of these equations provides the longitudinal chain order parameter

$$S_\theta = -0.5(S_x + S_y), \tag{4.1}$$

which serves as a measure of the segmential ordering and/or tilting of the chain long axes with respect to the membrane normal.

Figure 14 (part below) shows the longitudinal chain order parameter, S_θ, and the center of gravity of the symmetric methylene stretching band, COG ($\nu_s(CH_2)$), of fully hydrated dimyristoyl PC (DMPC) as a function

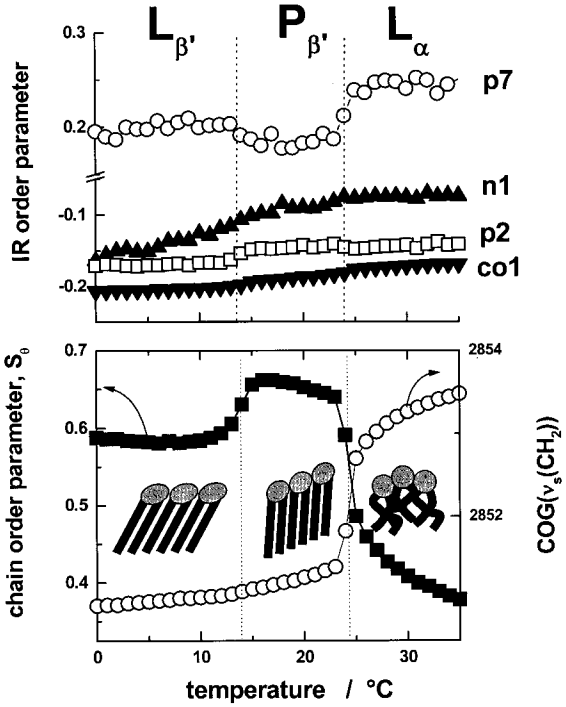

Figure 14. IR characteristics of hydrated DMPC as a function of temperature (RH = 100%). Part below: chain order parameter, S_θ (left ordinate), and centre of gravity of the $\nu_s(CH_2)$ vibration (right ordinate). Part above: IR order parameter of different vibrations of the polar part of DMPC (see Fig. and Table 2 for assignments). The phase transition temperatures between the tilted gel phase ($L_{\beta'}$), the ripple phase ($P_{\beta'}$) and the liquid crystalline (L_α) phase are indicated by vertical dotted lines.

of temperature. On heating, the lipid passes the phase sequence gel ($L_{\beta'}$) → ripple gel ($P_{\beta'}$) → liquid crystalline (L_α). In the gel phase the polymethylene chains exist in the extended all-trans conformation. Their long axes tilt with respect to the membrane normal. Upon transformation into the ripple phase S_θ distinctly increases whereas COG($\nu_s(CH_2)$) remains virtually constant. The invariance of the latter parameter indicates that the conformation of the chains only weakly changes at the $L_{\beta'}$ / $P_{\beta'}$ phase transition whereas the tilt angle of the chain long axes decreases as indicated by the alteration of the order parameter, S_θ (see also Eq. (3.20)). The subsequent chain melting transition between the ripple gel and the liquid crystalline phase is characterised by the parallel alterations of COG($\nu_s(CH_2)$) and S_θ. These tendencies reflect the decrease of segmential order owing to the appearance of gauche defects.

Selected IR order parameters of the PC headgroups and of the carbonyl group are also shown in Fig. 14 for comparison with the chain order parameter (see part above). Headgroup orientation and ordering are only weakly affected at the phase transitions.

T. Phase Transitions Between Lamellar and Nonlamellar Phases

Figure 15 shows the hydration dependence of the chain order parameter, S_θ, of di-oleoyl PC, DOPC. Upon decreasing RH, S_θ initially

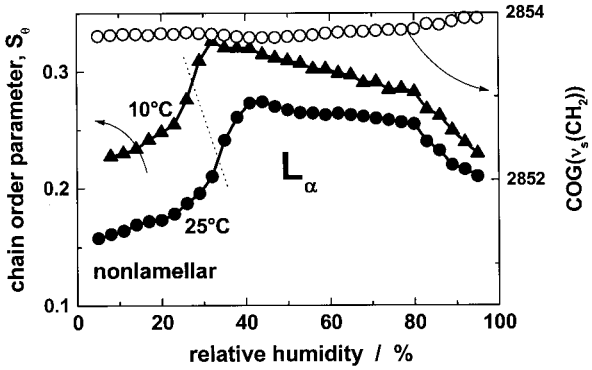

Figure 15. IR characteristics of DOPC as a function of relative humidity at $T = 10^\circ C$ and $25^\circ C$. The solid symbols refer to the chain order parameter, S_θ (left ordinate), and the open circles to the center of gravity of the $\nu_s(CH_2)$ vibration (right ordinate, $T = 25^\circ C$).

MARCEL DEKKER, INC. • 270 MADISON AVENUE • NEW YORK, NY 10016

increases owing to the dehydration-induced lateral compression of the membranes (vide supra). At a critical RH value the chain order parameter however distinctly decreases. The mean frequency of the symmetric methylene stretching band, $\nu_s(CH_2)$, is nearly a constant at all studied conditions (see open circles in Fig. 15). Its value is typical for molten acyl chains. Consequently the observed change of molecular order refers to a lyotropic transition between two fluid phases.

Let us introduce two geometrical parameters characterising in a simple fashion the balance of intermolecular forces in a membrane, namely the cross section of the headgroup (A_{head}) and of one chain (A_{chain}) in a plane parallel to the membrane surface. The stability criterium for a lamellar structure requires $A_{head} = 2A_{chain}$. Deviations from this condition cause a bending moment, which tends to transform the lamellae into a non-lamellar structure. Small deviations from the condition $A_{head} = 2A_{chain}$ are however balanced because the two bending moments in the two monolayers of the membrane compensate each other because they act into opposite directions. This situation holds, for example, for lipids with well-hydrated bulky headgrpoups and with at least one saturated chain such as DLPC, DMPC, DPPC and POPC. These lipids form exclusively lamellar phases at room temperature.

In lipids with relatively small, weakly hydrated headgroups, such as PEs, the cross section of the chains considerably exceeds that of the headgroup at reduced hydration, $A_{head} < 2A_{chain}$. In this case, the disbalanced forces cause the bending into nonlamellar, ''water-inside'' structures. For example, DOPE, forms exclusively nonlamellar H_{II} and P_α phases in the the respective hydration range (Fig. 6).

The PC analogue of DOPE, DOPC, clearly forms membranes in the fully hydrated state. Removal of water however induces the transition into a nonlamellar phase at a critical value of RH < 40%. This event is easily detected by means of IR linear dichroism because nonlamellar structures distinctly reduce the value of the IR order parameter of the lipid (see Eq. (3.16)). This result illustrates the capability of IR linear dichroism to detect phase transitions between lamellar and nonlamellar phases.

U. Polar Region: Phosphocholine and Carbonyl-ester Groups

Several closely spaced absorption bands overlap in the spectral region around 1000 cm^{-1} giving rise to a feature, which is characteristic for the polar part of a particular phospholipid. Most of the involved

bands in this fingerprint region can be assigned to ester-bond stretches of the C^G–O–P–O–C^C backbone of the phosphodiester group (the superscripts G and C refer to the glycerol and the choline moieties) and of the carbonyl-ester groups (see Table 2). Especially the identification and differentiation of the former modes is difficult. Note that the spectrum of the dichroic ratio, $R(\nu)$ (see Fig. 12), clearly reveals several overlapped modes, which can be hardly detect in the absorption spectra.

Figure 16 shows the polarised absorption spectra of POPC, of POPC-*d*4 with deuterated choline methylenes and a series of absorption spectra of methyl-PC, which are measured at increasing hydration. The position of vibrations, which involve the choline moieties are

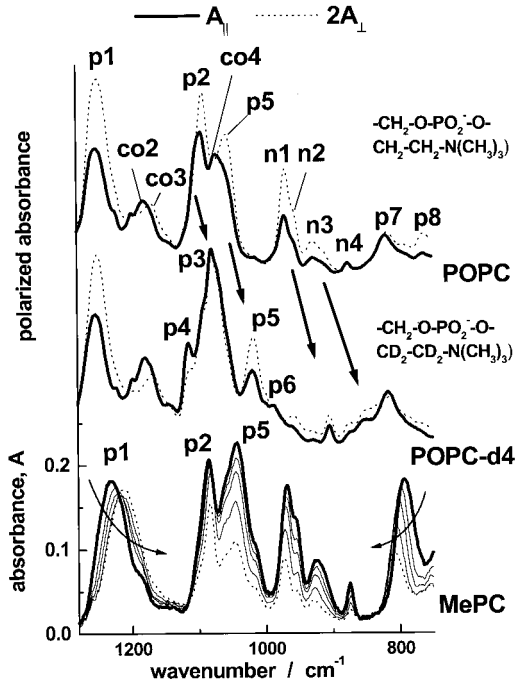

Figure 16. The "fingerprint" region of the IR spectrum of POPC (above), of headgroup-deuterated POPC-*d*4 (middle) and of methyl PC (below) mainly due to vibrations of the polar part of the lipids (see Table 2 for assignments). The arrows indicate the isotopic shift of vibrations, which involve the choline methylenes. The polarised spectra of POPC and of POPC-*d*4 were recorded at RH = 11% and $T = 25^{\circ}$C, respectively. The sum spectra of MePOC refer to increasing RH = 20% (thick solid line), 50, 65, 89, 98% (dotted line).

expected to differ in the spectra of POPC and of POPC-*d*4. Indeed, the rigth-hand shift of several bands by 30–50 cm^{-1} enables their assignment to P–O–C^C and C–N–$(CH_3)_3$ stretches (see also Table 2). The linear dichroism and the IR order parameter of the phosphodiester stretches can be explained by C^G–O–P and P–O–C^C fragments, which orient with their long axes more parallel and more perpendicular relative to the membrane normal, respectively (see also Fig. 13 for illustration).

Methyl-PC lacks carbonyl-ester groups. Consequently the comparison of the spectra of POPC and of methyl-PC allows the assignment of the C–O–C stretches. The dichroism of the symmetric modes (co2 and co3) in the spectrum of POPC reflects the different conformations and orientations of the acyl chains in the sn-1 and sn-2 position of diacyl lipids (see also Fig. 13). Interestingly, also the dichroic spectrum of the C=O stretching band clearly shows the existence of at least two subbands of different orientation (see Fig. 12, co1). The right-hand component near 1725 cm^{-1} can be attributed to a population of stronger hydrated carbonyls the C=O double bonds of, which point more parallel to the membrane plane. The C=O bonds of the left-hand component band near 1748 cm^{-1} orient slightly more in direction of the membrane normal. The bigger wavenumber suggests that the respective carbonyls are only weakly involved into hydrogen bonding.

Upon hydration the intensity of the spectrum of Me-PC decreases because the absorbing species are diluted in sorbed water. Note also the hydration-induced, characteristic shift of the phosphate modes p1 and p7 into opposite directions.

V. Interaction with Ions

Divalent cations specifically interact with the PC headgroups (see, Ref.[49] and references cited therein). The fingerprint region of the polarised absorbance spectra and the respective dichroic ratio of POPC in the gel state indicates considerable changes of headgroup conformation and orientation after addition of Ca^{2+} (compare Figs. 16, 17 and 18). Especially absorption bands due to vibrations of the C^G–O–P–O–C^C fragment (p3 to p6) considerably sharpen and reveal strong linear dichroism. These tendencies can be explained by the alteration of the backbone of the phosphodiester groups from a more disordered conformation to a uniform structure, which is characterised by a relatively narrow range of torsional angles for rotations about the respective ester bonds.

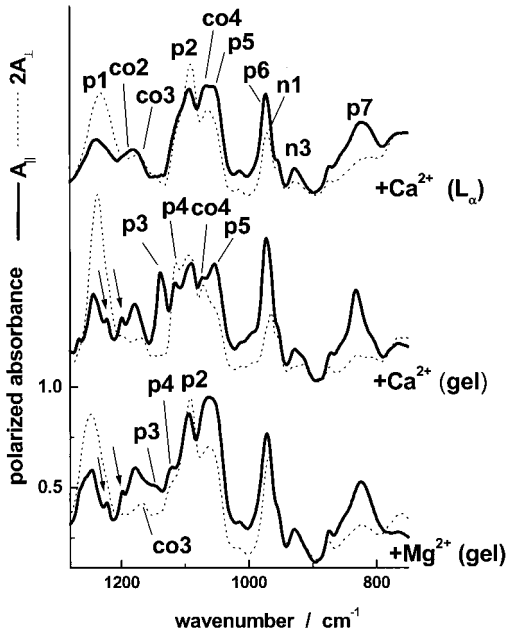

Figure 17. The "fingerprint" region of the IR spectrum of POPC in the liquid crystalline (above, RH = 77%) and gel (middle, RH = 47%) phase in the presence of $CaCl_2$, and in the presence of $MgCl_2$ (RH = 10%). The mole ratio lipid:metal chloride is 1:0.7. For assignments see Table 2. The arrows indicate components of the CH_2 wagging progression bands of the all-trans palmitoyl chains of the lipid.

The IR order parameters of the p7 mode of PC lipids is positive (i.e., $R(\nu) > 2$) and that of the p1 band is negative (i.e., $R(\nu) < 2$) in the absence and presence of Ca^{2+} as well (Fig. 18). This result indicates that the plane formed by the O–P–O atoms perpendicularly intersects the membrane surface on the average because the respective transition moments approximately point parallel and perpendicular with respect to the O–P–O plane, respectively. The preferred conformation of the C^G–O–P–O–C^C backbone is g (gauche)$^+/g^+$ or g^-/g^-.[12,50] For this situation the orientation the O–P–O group is not coplanar with the adjacent C^G–O–P and P–O–C^C fragments, which orient in an oblique fashion with respect to the membrane surface. The transition moments of p3 and p5 lie approximately within the P–O–C^C plane and that of p4 and p6 within the C^G–O–P plane. For an oblique orientation one expects IR order parameters ranging from slightly negative to slightly positive values in agreement with the observed data.

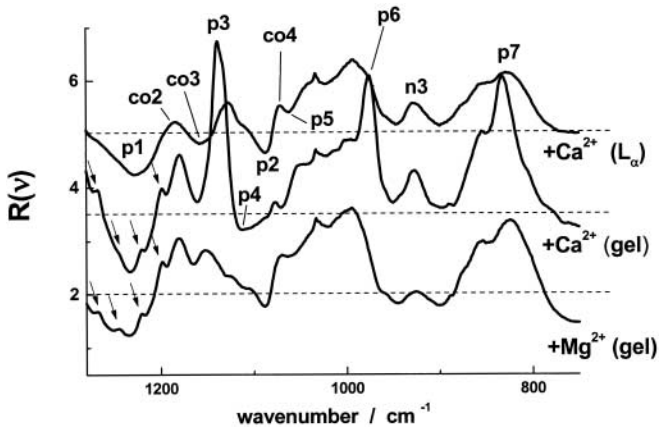

Figure 18. Spectrum of the dichroic ratio, $R(\nu) = A_{||}(\nu)/A_{\perp}(\nu)$), of the "fingerprint" region of the IR spectrum of POPC in the presence of Ca^{2+} and Mg^{2+}. $R(\nu)$ was calculated by means of the polarised spectra shown in Fig. 17. For assignments see Table 2. The arrows indicate components of the CH_2 wagging progression bands of the all-trans palmitoyl chains of the lipid. The $R(\nu)$ spectra in the part in the middle and above are shifted by an increment of 1.5 for clarity. The dashed lines refer to $R(\nu) = 2$.

The transition moments of the modes of p3, of p6 and partially of p5 strongly orient along the membrane normal after addition of Ca^{2+}. This tendency is compatible with the conformational change of the C^G–O–P–O–C^C backbone from g/g to *t*(trans)/*t*. The whole C^G–O–P–O–C^C–group becomes planar in this case. The strong parallel dichroism of the discussed vibrational bands can be understood if the plane formed by the C^G–O–P–O–C^C atoms intersects the membrane surface at the right angle. For negatively charged lipids such as dimyristoylphosphatidylserine or phosphatidic acid it is known that divalent metal ions induce a conformational change from the *g*/*g* to the *t*/*t* conformation upon binding to the phosphate groups.[51,52] Here a similar alteration of headgroup structure is suggested for PC headgroups in the presence of Ca^{2+}. Note also the marked linear dichroism of the vibrations n1, n2 and n3, which indicates a high degree of molecular order of the trimethylammonium group. The parallel dichroism of the in-plane (with respect to C–C–N) mode n1 indicates that the terminal C–C–N fragment and the C^G–O–P–O–C^C group orient predominantly coplanar.

The width of most of the considered bands increases in the liquid crystalline phase (see Figs. 17 and 18, part above). This tendency reflects

an higher conformational flexibility of the headgroups. The essential characteristics of the polarised spectra are however very similar in the solid and fluid phases indicating similar headgroup order (see, e.g., p5, p6 and n1). The disappearance of the strong p3 band in the dichroism spectrum reflects the increased mobility for rotations about the bonds in the P–O–C^C fragment and/or desorption of Ca^{2+} from a special binding site in this region. The latter hypothesis also provides an explanation for the much weaker intensity of p3 in the presence of Mg^{2+} (Figs. 17 and 18, part below). The smaller magnesium ions possibly occupy a different binding site compared with that of the bigger Ca^{2+} ions. The fact that the dichroism of the respective CO–O–C stretches, co3 and co4, differs between POPC + Ca^{2+} and POPC + Mg^{2+} in the gel state of the lipid lets us assume that this site is located deeper in the polar region more closely to the carbonyl ester group. The co3 band possesses strong parallel dichroism upon binding of Mg^{2+} probably due to a conformational change of the ester group in the sn-2 chain. It has been recently found that Mg^{2+} and Ca^{2+} increase the hydration degree of the carbonyl groups possibly because these moieties interact with the hydration shell of the ions.[49]

W. Hydration Complex of PC Headgroups

The chain melting transition of lipids is typically characterised by the sigmoidal change of two IR parameters, which sensitively respond to the conformational order of the chains, namely the position and the IR order parameter of the methylene stretching bands (see, e.g., Fig. 4). The respective IR characteristics of the di-C12 lipid DLPC differ from those of the other lipids with longer acyl chains. The mean wavenumber (Fig. 3) and the chain order parameter (Fig. 19, part below) of DLPC shift relatively continuously ($T > 15^\circ$C) or in two distinct steps ($T = 15^\circ$C). Polymethylene chains in the all-trans configuration give rise to the so-called methylene wagging band progression, a series of weak, equally-spaced, strongly parallel polarised absorption bands in the spectral range 1200–1340 cm^{-1}. Its existence provides an unambiguous spectral criterium for frozen all-trans chains. The methylene wagging bands of the C12 chains are clearly visible in the polarised $A_{||}(\nu)$ spectrum and in the spectrum of the dichroic ratio of DLPC at RH < 25% ($T = 25^\circ$C) and at RH < 75% ($T = 15^\circ$C, see Figs. 20 and 21). Consequently, the steplike changes of S_θ and COG($\nu_s(CH_2)$) at RH ≈ 25% ($T = 25^\circ$C) and at 75% ($T = 15^\circ$C) were clearly assigned to the respective chain melting transition.

MARCEL DEKKER, INC. • 270 MADISON AVENUE • NEW YORK, NY 10016

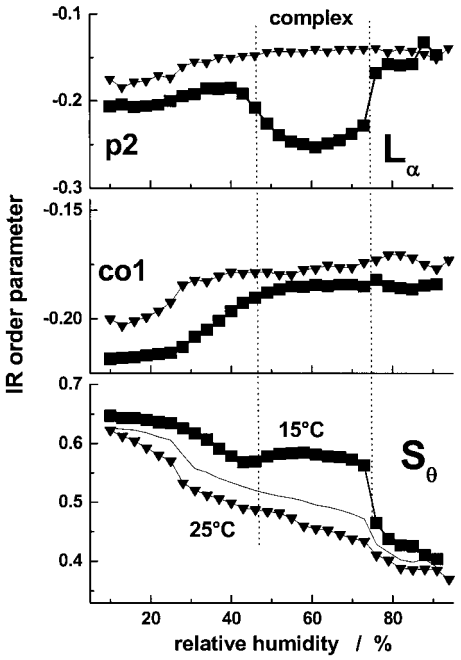

Figure 19. IR order parameters of DLPC as a function of RH at $T = 15^\circ C$ (squares), 20°C (solid line, part below) and 25°C (down triangles): chain order parameter calculated by means of the IR order parameters of the methylene stretches (S_θ, cf. Eq. (4.1), part below), S_{IR} of the carbonyl stretching band (co1, part in the middle) and of the $\nu_s(PO_2^-)$ band (p2, part above). The vertical dotted lines indicate the existence range of the water–lipid complex ($T = 15^\circ C$).

The adsorption isotherm of DLPC reveals a plateau in the RH range, which precedes the lyotropic chain melting transition ($45\% < RH < 75\%$, see Fig. 3). The virtually constant number of water molecules per lipid, $R_{W/L} \approx 2.5$, indicates the existence of a stochiometric water-lipid complex. At the lyotropic chain melting transition each lipid molecule imbibes 2–3 water molecules as indicated by the steep increase of $R_{W/L}$, which accompanies the stepwise increase of the mean wavenumber of the $\nu_s(CH_2)$ band near $RH \approx 75^\circ C$ (Fig. 3).

The complex is characterised by a marked drop of the infrared order parameter of the $\nu_s(PO_2^-)$ (p2, Fig. 19, part above) and of the $\nu_{as}(PO_2^-)$ (p1, not shown) bands indicating a reorientation in the polar part of DLPC. Note that the IR order parameters of other modes such as $\nu(C{=}O)$ (co1, Fig. 19) and of $\nu_{as}(P(OC)_2^-)$ (p7, not shown) are virtually

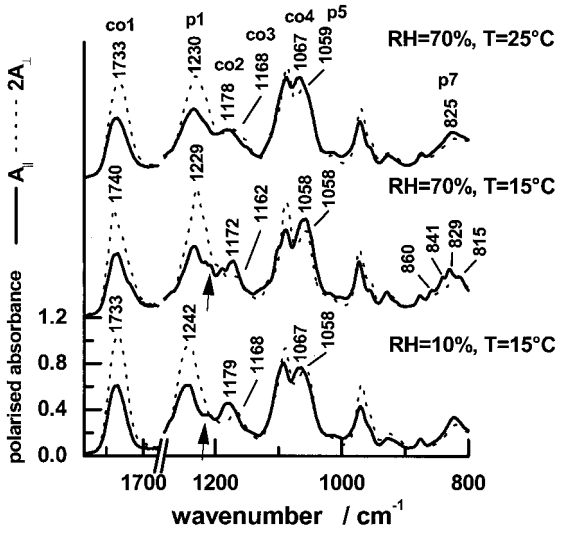

Figure 20. Polarised IR spectra of DLPC. The respective conditions (temperature and RH) are given in the figure together with the peak position of selected absorption bands (in units of cm^{-1}), which are assigned in the upper part of the figure and in Table 2. The arrows indicate the first band of the methylene wagging progression of the all-trans C12 chains near 1206 cm^{-1} ($T = 15°C$, part in the middle and below).

not affected by complex formation. No evidence of complex formation was detected at $T = 25°C$.

Inspection of the polarised spectra in the RH range of the hydration complex reveals interesting structural properties of the polar part of DLPC (Figs. 20 and 21, $T = 15°C$, RH = 70%): (i) The $\nu_{as}(P–(OC)_2)$ band (p7) splits into at least four subbands. This effect indicates that the $C^G–O–P–O–C^C$ backbone exists in a rigid state. The appearance of the component bands of different linear dichroism can be either due to factor group splitting in a crystalline arrangement of the phosphate groups, to different interaction modi of the esterified oxygens and/or to different conformations of the $C^G–O–P–O–C^C$ backbone. (ii) Also the C=O stretching vibration (co1) splits into strongly polarised subbands, which reflect a rigid structure of the carbonyl groups. Two more parallel bands at 1742 and 1724 cm^{-1} alternate with more perpendicular ones at 1732 and 1713 cm^{-1}. (iii) The antisymmetric CO–O–C stretching band of the lauroyl chains in the sn-1 position (co2) shifts by 5–8 cm^{-1} towards smaller wavenumbers compared with its usual position in di-acyl PCs

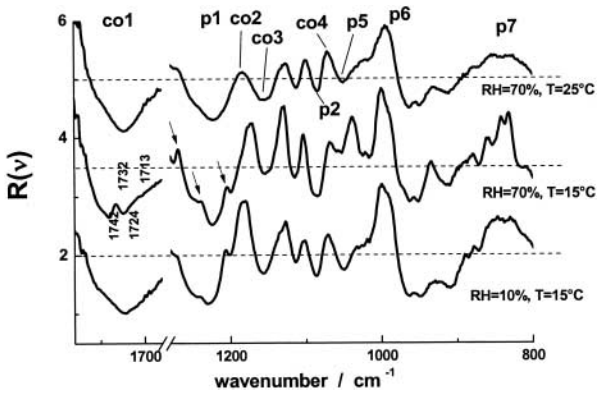

Figure 21. Spectrum of the dichroic ratio, $R(\nu) = A_{||}(\nu)/A_{\perp}(\nu)$), of the "fingerprint" region of the IR spectrum of DLPC. $R(\nu)$ was calculated by means of the polarised spectra shown in Fig. 20. For assignments see Table 2. The arrows indicate components of the CH_2 wagging progression bands of the all-trans lauroyl chains of the lipid. They possess strong parallel dichroism. The $R(\nu)$ spectra in the middle and above are shifted by an increment of 1.5 for clarity. The dashed lines refer to $R(\nu) = 2$.

(vide supra and DLPC at $T = 25°C$). The virtual invariance of the dichroism of the co2 band lets us suggest that the observed spectral shift is mainly due to altered interactions of the carbonyl-ester groups and to a less extend to a conformational change of this moiety. Note that the shift of the co2 band is paralleled by a similar shift of the respective symmetric mode (co4). The effects (ii) and (iii) show that a certain fraction of carbonyl-ester groups exist in a specific state in the considered RH range, which is correlated with a rigid structure of the phosphodiester groups (effect (i)). The water-lipid complex obviously involves the carbonyl- and phosphodiester groups. On the other hand, the mean position of the $\nu_{as}(PO_2^-)$ band (co1) shifts nearly continuosly also in the RH range in, which $R_{W/L}$ is nearly a constant (see Fig. 3). This fact shows that the structure and the interactions within the complex vary with the water activity.

Note that also the adsorption isotherm of DMPC implys the formation of a stochiometric water-lipid complex in the mid-RH range whereas the isotherm of DPPC gives no indication (see Fig. 3). Analysis of the polarised IR spectra of DMPC does not reveal structural changes of the polar part comparable to that observed upon complex formation of DLPC (not shown). Hence, the tendency of complex formation with consequences for the structure of the polar part decreases with increasing chain

length according to the sequence DLPC > DMPC > DPPC. The particular molecular arrangement represents an optimization of the partially incompatible requirements for maximal *van der Waal's* contacts between the hydrocarbon chains and for maximal polar interactions at the headgroups and polar/apolar interfacial regions of the lipid bilayer. Longer chain PCs exhibit less extensive hydrogen-bonding interactions at the polar/apolar interface but a tighter packing of the hydrocarbon chains than the corresponding short chain homologues. The latter are characterised by the more extensive hydration but the relatively loose packing of the acyl chains. These opposite tendencies are clearly reflected in the IR characteristic shown in Fig. 3 for DLPC, DMPC and DPPC: The mean wavenumber of the $\nu_{as}(PO_2^-)$ band systematically increases for longer chains (at RH = const) whereas that of $\nu_s(CH_2)$ systematically decreases indicating weaker hydration of the phosphate groups and the more effective packing of the chains, respectively. Upon formation of the hydration complex of DLPC the water/lipid interactions apparently overcome the *van der Waal's* forces acting in the hydrophobic core of the bilayer and thus determine the molecular arrangement. For the PCs with longer acyl chains such as DMPC and DPPC the relation reverses: chain packing becomes more important and determines the structure of the membrane.

X. Oriented Water

The water adsorbed to the lipid gives rise to a broad absorption band in the spectral range 3700–3000 cm^{-1} due to a variety of O–H stretching modes, $\nu_{13}(H_2O)$ (Fig. 22). Its position and shape depend on several factors such as the distribution of hydrogen bonds of variable strength over a variety of binding sites and on the degree of intramolecular and intermolecular vibrational coupling within the particular water structure.[53–55] The IR spectrum of the primary hydration shell of DLPC shows two distinct peaks near 3390 cm^{-1} and 3250 cm^{-1}, which are due to water molecules in an effective H-bonded structure (''lattice water'').[55] The right-hand, less intense band can be assigned to a mode where symmetric ν_1 stretches of neighboring water molecules couple in-phase.[56,57] The left-hand band is assumed to originate from a complex mixture of different modes with a major fraction of antisymmetric H_2O stretches (ν_3) and a minor fraction of symmetric ν_1 stretches of water molecules, which couple out-of phase. A weak shoulder near 3600 cm^{-1} was assigned to non- or weakly hydrogen-bonded water.[55] The primary hydration shell of water, which binds to DLPC obviously forms well

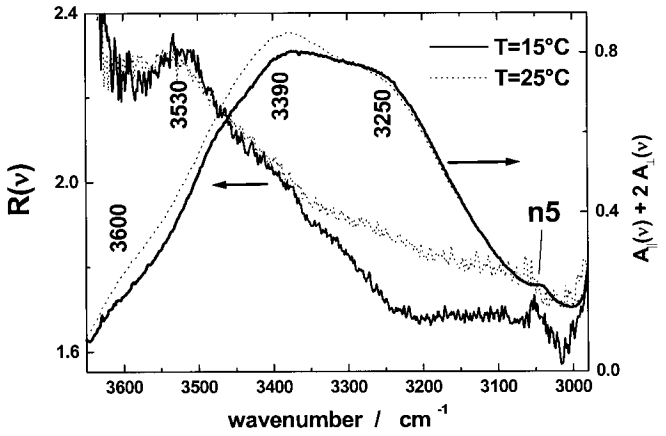

Figure 22. Absorption spectrum (right ordinate, see arrow) and spectrum of the dichroic ratio (left ordinate) of the water adsorbed to DLPC at RH = 70% and $T = 15^{\circ}C$ (gel state) and $25^{\circ}C$ (liquid crystalline state, see figure for assignments). The numbers give characteristic wavenumbers in units of cm^{-1} (see text).

structured H-bonds, preferentially to the phosphate and carbonyl-ester groups as indicated by the relatively intense band at $3250\,cm^{-1}$ (Fig. 22).[34] Upon transformation of the lipid into the fluid state its relative intensity decreases whereas the intensity of the shoulder at $3600\,cm^{-1}$ increases. A certain fraction of structurated "lattice water" obviously transforms into non-bound water at the chain melting transition.

The spectrum of the dichroic ratio indicates that the dichroism changes across the wavenumber range of the ν_{13}(OH) band from $R(\nu) > 2$ at wavenumbers greater than $3390\,cm^{-1}$ to $R(\nu) < 2$ at smaller frequencies (Fig. 22). According to our previous analysis it is reliable to assume that the low wavenumber flank of the ν_{13}(OH) band refers to a "ν_1-like" mode whereas the high wavenumber flank originates from a "ν_3-like" mode.[36] The dichroism of the former mode reflects the average orientation of the symmetry axis of the water molecules.

We calculate the IR order parameters $S_{IR}(\nu_{3550})$ and $S_{IR}(\nu_{3250})$ in restricted spectral ranges at higher ($3550 \pm 20\,cm^{-1}$) and lower ($3250 \pm 20\,cm^{-1}$) wavenumbers, respectively, to estimate the molecular order of water adsorbed to DLPC (Fig. 23) and DMPC (Fig. 24). The transition moment of the "ν_1-like" mode roughly points along the bisector of the H–O–H bond angle. Consequently, $S_{IR}(\nu_{3250})$ provides a measure of the orientation of the water dipole moment relatively to the membrane normal. This order parameter sensitively responds to structural changes of

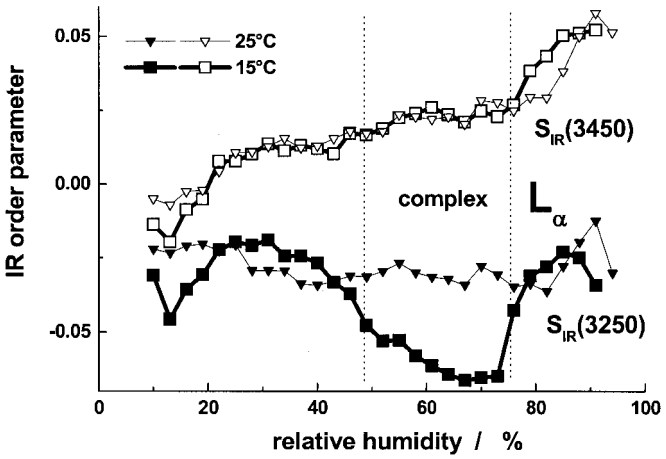

Figure 23. IR order parameter of water adsorbed to DLPC at $T = 15^{\circ}C$ and $25^{\circ}C$ as a function of RH. The IR order parameters $S_{IR}(\nu_{3550})$ and S_{IR} (ν_{3250}) refer to the left-hand and right-hand flank of the $\nu_{13}(H_2O)$ band shown in Fig. 22 (see text). The vertical dotted lines border the RH range of the water–lipid complex ($T = 15^{\circ}C$).

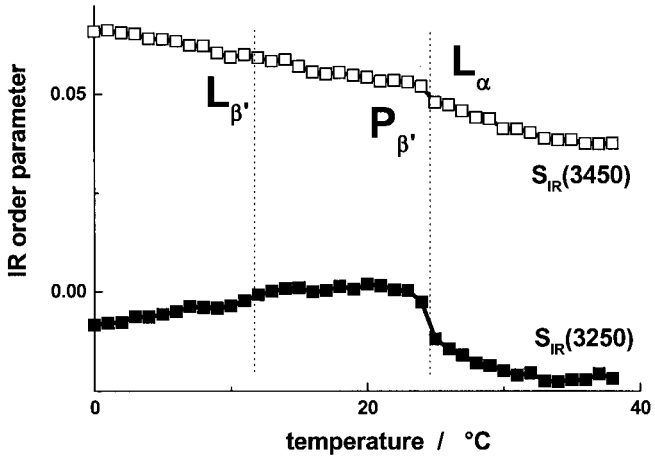

Figure 24. IR order parameter of water adsorbed to fully hydrated DMPC as a function of temperature. The vertical dotted lines indicate the phase transitions (see also Fig. 14).

the lipids such as the formation of the hydration complex of DLPC (Fig. 23) and the thermotropic chain melting transition of fully hydrated DMPC (Fig. 24). The decrease of $S_{IR}(\nu_{3250})$ in the RH range of complex formation of DLPC and at the gel-to-liquid crystalline phase transition of DMPC is compatible with a more parallel alignment of the water dipoles with respect to the membrane plane. The IR order parameter of the H_2O scissoring band near $1650\,cm^{-1}$ ($\delta(H_2O)$) changes in a similar fashion as $S_{IR}(\nu_{3250})$ (data not shown). This result confirms the hypothesis about the orientation of the transition moment of $S_{IR}(\nu_{3250})$ because also the transition moment of $\delta(H_2O)$ is assumed to point in direction of the water dipole. The water order parameter $S_{IR}(\nu_{3250})$ similarly changes as selected IR order parameters of the phosphate group, namely that of p2 of DLPC (compare Fig. 19, part above, and Fig. 23) and that of p7 of DMPC (compare Fig. 14, part above, and Fig. 24). The mean orientation of water dipoles and the ordering and orientation of the phosphate group are tightly correlated whereas the mean orientation of the carbonyl groups behaves in a different fashion.

The order parameter of the "ν_3-like" mode, $S_{IR}(\nu_{3450})$, is assumed to reflect the mean orientation of the "water-planes" formed by the H–O–H atoms with respect to the membrane normal because the respective transition moment roughly points along the interconnecting line between both water hydrogens. Interestingly, this order parameter does virtually not respond to the structural changes of the lipids discussed above. Instead it continuously changes over the studied RH and T ranges. These results give rise to the conclusion that dipolar interactions and H-bonds to the phosphate groups determine the order of water near the membrane.

V. SUMMARY AND CONCLUSIONS

1. The adjustment of the hydration degree of materials by means of the **humidity titration technique** has proved to be practical, relatively fast to achieve, accurate, and, last but not least, well-defined in a thermodynamic sense. The method is called humidity titration because "gaseous water" is "injected" in definite portions of the relative humidity into the sample chamber.
2. In combination with **ATR infrared spectroscopy** this technique is well suited to explore hydration-induced phenomena in amphiphilic systems. One special advantage of humidity-tuned infrared spectroscopy should be recognized in its capacity for the parallel investigation of several aspects of lipid hydration. Information about intermolecular interactions, conformational

changes and other structural aspects in different parts of the molecules can be studied within one experiment.

3. Infrared **linear dichroism** spectroscopy is a powerful tool to investigate the architecture of amphiphilic aggregates on a molecular level because the spectral information about molecular conformations and interactions is supplemented by informations about molecular orientation. Linear dichroism measurements are shown to detect alterations of aggregate morphology with high sensitivity. Furthermore, they improve the spectral resolution in the spectral range of band overlaps.
4. Investigations at **variable hydration** provide a direct approach to molecular interactions, which depend directly on intermolecular distances and molecular conformations. The phase state and the particular packing of amphiphilic molecules are affected not only by the nature of the polar part, but also by its apolar part, which, in turn, modify the potency of the system to bind water. Hydration studies are relevant because they probe the **material properties** of biological-relevant structures such as lipid membranes, which are highly anisotropic on a microscopic lengthscale.
5. A further field of application can be seen in the study of the **effect of additives** such as proteins, model peptides, sugars, anesthetics and cholesterol on membrane architecture and hydration. These compounds can modify the interaction pattern in the polar interface leading to different hydration properties of the mixed membranes with consequences for structure and biological function.

ACKNOWLEDGMENTS

I thank B. Kohlstrunk for the perfect realisation of the humidity technique and W. Pohle for cooperation, valuable comments and helpful discussion about many questions around hydration phenomena.

REFERENCES

1. Binder, H.; Schmiedel, H. Infrared dichroism investigations on the acyl chain ordering in lamellar structures I. The formalism and its application to polycrystalline stearic acid. Vibrational Spectroscopy **1999**, *21*, 51–73.

2. Binder, H.; Anikin, A.; Lantzsch, G.; Klose, G. Lyotropic phase behavior and gel state polymorphism of phospholipids with terminal diene groups. Infrared measurements on molecular ordering in lamellar and hexagonal phases. J. Phys. Chem. B **1999**, *103*, 461–471.
3. Binder, H.; Pohle, W. Structural aspects of lyotropic solvation-induced transitions in phosphatidylcholine and phosphatidylethanolamine assemblies revealed by infrared spectroscopy. J. Phys. Chem. B **2000**, *104*, 12039–12048.
4. Casal, H.L.; Mantsch, H.H. Polymorphic phase behavior of phospholipid membranes studied by infrared spectroscopy. Biochim. Biophys. Acta **1984**, *779*, 381–401.
5. Michl, J.; *Thulstrup Spectroscopy with Polarized Ligh*t; VCH Publishers: New York, 1986.
6. Holland, R.F.; Nielsen, J.R. Infrared spectra of single crystals, part I. Orthorhombic *n*-$C_{24}H_{50}$, Monoclinic *n*-$C_{36}H_{74}$, and Triclinic *n*-$C_{18}H_{38}$ and *n*-$C_{20}H_{42}$. J. Mol. Spectroscopy **1962**, *8*, 383–405.
7. Saupe, A.; Maier, W. Methoden zur bestimmung des ordnungsgrades nematischer kristallinflüssiger schichten. Z. Naturf. **1961**, *16a*, 816–824.
8. Kiefer, R.; Baur, G. Molecular biaxiality in nematic liquid crystals as studied by infrared dichroism. Mol. Cryst. Liq. Cryst. **1989**, *174*, 101–126.
9. Harrick, N.J. *Internal Reflection Spectroscopy*; Wiley: New York, 1967.
10. Fringeli, U.P.; Müldner, H.G.; Günthard, H.H.; Gasche, W.; Leuzinger, W. The structure of lipids and proteins studied by attenuated total-reflection (ATR) infrared spectroscopy. I. Oriented layers of tripalmitin. Z. Naturf. **1972**, *27b*, 780–796.
11. Fringeli, U.P. The structure of lipids and proteins studied by attenuated total-reflection (ATR) infrared spectroscopy. II. Oriented layers of a homologous series: phosphatidylethanolamine to phosphatidylcholine. Z. Naturf. **1977**, *32c*, 20–45.
12. Fringeli, U.P.; Günthard, H.H. Infrared membrane spectroscopy. molecular biology. Biochemistry and Biophysics **1981**, *31*, 270–332.
13. Ter-Minassian-Saraga, L.; Okamura, E.; Umemura, J.; Takenaka, T. Fourier transform infrared-attenuated total reflection spectroscopy of hydration of dimyristoylphosphatidylcholine multibilayers. Biochim. Biophys. Acta **1988**, *946*, 417–423.
14. Okamura, E.; Umemura, J.; Takenaka, T. Orientation studies of hydrated dipalmitoylphosphatidylcholine multibilayers by polarized FTIR-ATR spectroscopy. Biochim. Biophys. Acta **1990**, *1025*, 94–98.

15. Hübner, W.; Mantsch, H.H. Orientation of specifically $^{13}C{=}O$ labeled phosphatidylcholine multilayers from polarized attenuated total reflection FT-IR spectroscopy. Biophys. J. **1991**, *59*, 1261–1272.
16. Wenzl, P.; Fringeli, M.; Goette, J.; Fringeli, U.P. Supported phospholipid bilayers prepared by the ''LB/attenuated method'': a fourier transform infrared attenuated total reflection spectroscopic study on structure and stability. Langmuir **1995**, *10*, 4253–4264.
17. Tamm, L.; Tatulian, S. Infrared spectroscopy of proteins and peptides in lipid bilayers. Quart. Rev. Biophys. **1997**, *30*, 365–429.
18. Guo, J.D.; Zerda, T.W. Raman study on effects of high pressure on the structure of DPPC-cholesterol multilamellar vesicles. J. Phys. Chem. B **1997**, *101*, 5490–5496.
19. Siminovitch, D.J.; Wong, P.T.T.; Mantsch, H.H. Effects of cis and trans unsaturation on the structure of phospholipid bilayers: a high-pressure infrared spectroscopic study. Biochemistry **1987**, *26*, 3277–3287.
20. Wong, P.T.T.; Siminovitch, D.J.; Mantsch, H.H. Structure and properties of model membranes: new knowledge from high-pressure vibrational spectroscopy. Biochim. Biophys. Acta **1988**, *947*, 139–171.
21. Winter, R.; Czeslik, C. Pressure effects on the structure of lyotropic lipid mesophases and model biomembrane systems. Z. Kristallogr. **2000**, *215*, 454–474.
22. Parsegian, V.A.; Fuller, N.; Rand, R.P. Measured work of deformation and repulsion of lecithin bilayers. Proc. Natl. Acad. Sci. USA **1979**, *76*, 2750–2754.
23. Koenig, B.W.; Strey, H.H.; Gawrisch, K. Membrane lateral compressibility measured by NMR and X-ray diffraction. Biophys. J. **1997**, *73*, 1954–1966.
24. Binder, H.; Dietrich, U.; Schalke, M.; Pfeiffer, H. Hydration induced deformation of lipid aggregates before and after polymerization. Langmuir **1999**, *15*, 4857–4866.
25. Binder, H.; Anikin, A.; Kohlstrunk, B.; Klose, G. Hydration induced gel states of the dienic lipid 1,2-*bis*(2,4-octadecanoyl)-Sn-glycero-3phosphorylcholine and their characterization using infrared spectroscopy. J. Phys. Chem. B **1977**, *101*, 6618–6628.
26. Rand, R.P.; Parsegian, V.A. Hydration forces between phospholipid bilayers. Biochim. Biophys. Acta **1989**, *988*, 351–376.
27. Young, J.F. Humidity control in the laboratory using salt solutions—A review. J. Appl. Chem. **1967**, *17*, 241–245.
28. Pohle, W.; Selle, C.; Fritzsche, H.; Binder, H. Fourier transform infrared spectroscopy as a probe for the study of the hydration of

lipid self-assemblies. I. Methodology and general phenomena. Biospectroscopy **1998**, *4*, 267–280.
29. Wadsö, L.; Markova, N. A double twin isothermal microcalorimeter. Thermochim. Acta **2000**, *360*, 101–107.
30. Binder, H.; Kohlstrunk, B.; Pohle, W. Thermodynamic and kinetic aspects of lyotropic solvation-induced transitions in phosphatidylcholine and phosphatidylethanolamine assemblies revealed by humidity titration calorimetry. J. Phys. Chem. B **2000**, *104*, 12049–12055.
31. Binder, H.; Kohlstrunk, B. Infrared dichroism investigations on the acyl chain ordering in lamellar structures II. The effect of diene groups in membranes of dioctadecadienoylphosphatidylcholine. Vibrational Spectroscopy **1999**, *21*, 75–95.
32. Binder, H.; Kohlstrunk, B.; Heerklotz, H.H. A humidity titration calorimetry technique to study the thermodynamics of hydration. Chem. Phys. Lett. **1999**, *304*, 329–335.
33. Binder, H.; Gawrisch, K. Dehydration induces lateral expansion of membranes of polyunsaturated 18:0–22:6 phosphatidylcholine in a new lamellar phase. Biophys. J. **2001**, *81*, 969–982.
34. Binder, H.; Kohlstrunk, B.; Heerklotz, H.H. Hydration and lyotropic melting of amphiphilic molecules-a thermodynamic study using humidity titration calorimetry. J. Coll. Interface Sc. **1999**, *220*, 235–249.
35. Binder, H.; Arnold, K.; Ulrich, A.S.; Zschörnig, O. Interaction of Zn^{2+} with phospholipid membranes. Biophys. Chem. **2001**, *90*, 57–74.
36. Binder, H.; Gutberlet, T.; Anikin, A.; Klose, G. Hydration of the dienic lipid dioctadecadienoylphosphatidylcholine in the lamellar phase-an infrared linear dichroism and X-ray study on headgroup orientation, water ordering and bilayer dimensions. Biophys. J. **1998**, *74*, 1908–1923.
37. Pohle, W.C.S.; Fritzsche, H.; Bohl, M. Comparative FTIR spectroscopic study upon the hydration of lecithins and cephalins. J. Mol. Structure **1997**, *408/409*, 273–277.
38. Binder, H.; Gawrisch, K. Effect of unsaturated lipid chains on dimensions, molecular order and hydration of membranes. J. Phys. Chem. B **2001**, *105*, 12378–12390.
39. Hung, W.C.; Chen, F.Y.; Huang, H.W. Order-disorder transition in bilayers of diphytanoylphosphatidylcholine. Biochim. Biophys. Acta **2000**, *1467*, 198–206.
40. Binder, H. Infrared dichroism investigations on the acyl chain ordering in lamellar structures III. Characterisation of the chain

tilt and biaxiality in the solid phases of dipalmitoylphosphatidylcholine as a function of temperature and hydration using molecular order parameters. Vibrational Spectroscopy **1999**, *21*, 151–163.
41. Katsaras, J. Adsorbed to a rigid substrate, dimyristoylphosphatidylcholine multibilayers attain full hydration in all mesophases. Biophys. J. **1998**, *75*, 2157–2162.
42. Becker, K.D. *Ausbreitung Elektro-Magnetischer Wellen*; Springer-Verlag: Berlin, 1974.
43. Binder, H.; Schmiedel, H.; Lantzsch, G.; Cramer, C.; Klose, G. Molecular ordering in microconfined liquid crystals: an infrared linear dichroism study. Liquid Crystals **1996**, *21*, 415–426.
44. Wu, S.-T. Infrared markers for determining the order parameters of uniaxial liquid crystals. Appl. Optics **1987**, *26*, 3434–3440.
45. Binder, H.; Gutberlet, T.; Anikin, A. Biaxial ordering of terminal diene groups in lipid membranes—an infrared linear dichroism study. J. Mol. Structure **1999**, *510*, 115–131.
46. Binder, H.; Kohlstrunk, B.; Brenn, U.; Schwieger, W.; Klose, G. Infrared dichroism measurements on the alkyl chain packing of an ionic detergent intercalated between silicate layers. Colloid Polym. Sci. **1998**, *276*, 1098–1109.
47. Derreumaux, P.; Wilson, K.J.; Vergoten, G.; Peticolas, W.L. Conformational studies of neuroactive ligands. 1. Force field and vibrational spectra of crystalline acetylcholine. J. Phys. Chem. **1989**, *93*, 1338–1350.
48. Tasumi, M.; Shimanouchi, T. Crystal vibrations and intermolecular forces of polymethylene crystals. J. Chem. Phys. **1965**, *43*, 1245–1257.
49. Binder, H.; Zschörnig, O. The effect of metal cations on the phase behavior and hydration characteristics of phospholipid membranes. Chem. Phys. Lipids **2002**, *115*, 39–61.
50. Hauser, H.; Guyer, W.; Spiess, M.; Pascher, I.; Sundell, S. The polar group conformation of a lysophosphatidylcholine analogue in solution—a high-resolution magnetic resonance study. J. Mol. Biol. **1980**, *137*, 265–282.
51. Casal, H.L.; Mantsch, H.H.; Hauser, H. Infrared studies of fully hydrated saturated phosphatidylserine bilayers . Effect of Li^+ and Ca^{2+}. Biochemistry **1987**, *26*, 4408–4416.
52. Laroche, G.; Dufourc, E.J.; Dufourcq, J.; Pezolet, M. Structure and dynamics of dimyristoylphosphatidic acid/calcium complexes by 2H NMR, infrared, and raman spectroscopies and small-angle X-ray diffraction. Biochemistry **1991**, *30*, 3105–3114.
53. Bertie, J.E.; Whalley, E. Infrared spectra of ices Ih and Ic in the range 4000 to 350 cm^{-1}. J. Chem. Phys. **1964**, *40*, 1637–1645.

54. Bertie, J.E.; Whalley, E. Infrared spectra of ices II, III, and V in the range 4000–350 cm^{-1}. J. Chem. Phys. **1964**, *40*, 1646–1659.
55. Walrafen, G.E. Raman spectral studies of the effects of temperature on water structure. J. Chem. Phys. **1967**, *47*, 114–127.
56. McGRaw, R.; Madden, W.G.; Bergren, M.S.; Rice, S.A.; Sceats, M.G. A theoretical study of the OH-stretching region of the vibrational spectrum of ice Ih. J. Chem. Phys. **1978**, *69*, 3483–3495.
57. Bergren, M.S.; Schuh, D.; Sceats, M.G.; Rice, S.A. The OH-stretching region infrared spectra of low density amorphous solid water and polycrystalline ice Ih. J. Chem. Phys. **1978**, *69*, 3477–3482.

MARCEL DEKKER, INC. • 270 MADISON AVENUE • NEW YORK, NY 10016